Eindhoven University of Technology

MASTER

Determination of mechanical properties of adherent cell types using the capillary micromechanics method

Doomen, Thomas A.J.W.

Award date:
2018

Link to publication

Disclaimer
This document contains a student thesis (bachelor's or master's), as authored by a student at Eindhoven University of Technology. Student theses are made available in the TU/e repository upon obtaining the required degree. The grade received is not published on the document as presented in the repository. The required complexity or quality of research of student theses may vary by program, and the required minimum study period may vary in duration.

General rights
Copyright and moral rights for the publications made accessible in the public portal are retained by the authors and/or other copyright owners and it is a condition of accessing publications that users recognise and abide by the legal requirements associated with these rights.

- Users may download and print one copy of any publication from the public portal for the purpose of private study or research.
- You may not further distribute the material or use it for any profit-making activity or commercial gain

TU/e - Microsystems
Eindhoven, May 7, 2018

Master thesis

"Determination of mechanical properties of adherent cell types using the capillary micromechanics method"

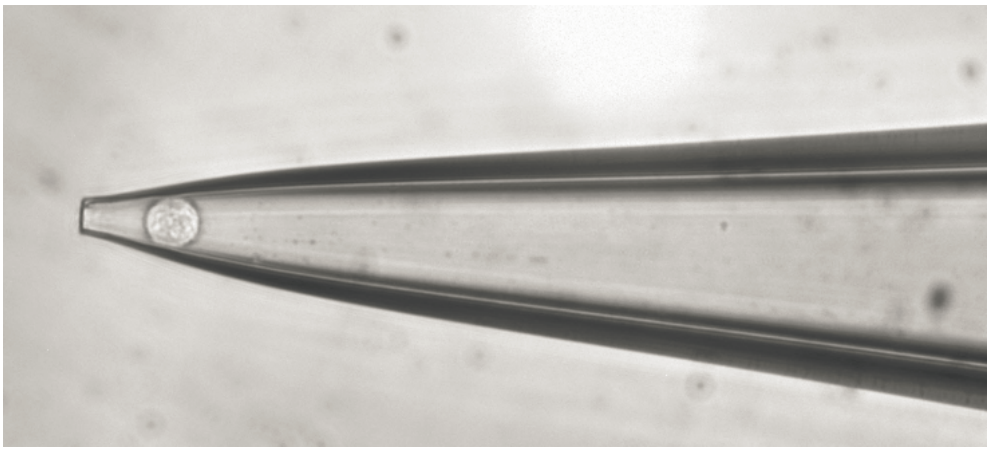

Master/department: Mechanical engineering

Research group: Microsystems

Author: T.A.J.W. Doomen

ID number: 0778968

s-number: s118402

Supervisors TU/e: S. SahebAli MSc

dr. H.M. Wyss

prof.dr.ir. J.M.J. den Toonder

Committee: S. SahebAli MSc

dr. H.M. Wyss

prof.dr.ir. J.M.J. den Toonder

dr. N.A. Kurniawan

1 Abstract

Knowledge about mechanical properties of single cells can play an important role in diagnosis and treatment. The mechanical properties can be used as so called biomarkers to recognize specific cell states and for understanding specific disease phases. For example for the invasion of cancer cells through tissue and vessel walls during the metastasis phase, the mechanical properties of cancer cells are expected to be important.

In the current study, the main focus was put on the determination of the mechanical properties of MDA-MB-231 cells. Additionally MCF-7 cells were studied to compare the mechanical properties. Both are breast cancer cell lines that had been used in previous cell invastion studies as model cell lines. The capillary micromechanics method was used to quantitatively determine the shear and compression modulus of these cells, with the challenge that both cell lines have adherent behaviors. The goal was to understand the invasion behavior which was observed in a previous study in a better way based on the determined moduli values.

During the capillary micromechanics measurements, single cells were deformed in a tapered capillary with a tip diameter of $\pm$ seven micrometers. Each cell was deformed in the capillary as a result of small pressure steps created with a fluid height difference, and images were made of each situation. With the use of image analysis, multiple strain values, pressure balances and finally values for the shear and compression modulus were determined for each measured cell. For the MDA-MB-231 cell line most of the times a strain stiffening behavior was observed, implying lower modulus values at small deformations compared to higher deformations. During the investigation also time dependency and the occurrence of elasto-plastic behavior were investigated. Finally it was possible to combine multiple measurements and to determine average modulus values as well as their standard deviations, as a measure of the mechanical properties of these cell lines. The results indicate significantly higher shear and compression moduli for the MDA-MB-231 cell line compared to the MCF-7 cell line. However, more measurements are needed to gain more insight into specific characterization of the MCF-7 cell line.

Contents

2 Introduction

In this investigation mechanical properties of the adherent MDA-MB-231 and MCF-7 cell types are determined using the capillary micromechanics method, and differences between these cell types in terms of the mechanical properties are discussed. To understand the importance and possibilities of mechanical property measurements of cells, it is first explained how mechanical properties are coupled to disease diagnosis and disease treatment, followed by listing multiple ways to determine the mechanical properties of cells including their advantages and disadvantages. Then the structure of cells related to their mechanical behavior is introduced and finally the project goal is given and the topics covered within this report are summarized.

2.1 Cell mechanics related to disease treatment

About 200 types of cells can be found which are responsible for all the biological functions within the human body[1]. To fulfill these biological functions each cell type has a specific size and shape, and specific physical and mechanical properties. When a cell type is subjected to a disease or a disease phase or when a diseased cell type is subjected to a chemical treatment, the cell behavior and the specific celltype properties may change. To diagnose and/or treat diseases or disease phases, so called biomarkers can be used. Biomarkers are measurable alterations of the human body or parts of the human body like cells, tissues, organs and fluids to indicate changes within the human body[2]. Examples of biomarkers are the presence and/or concentrations of proteins and antigens, the blood-sugar level for diabetes and the prostate specific antigen for the detection of prostate cancer[3]. Instead of focussing on the physiological behavior of diseases, disease phases or changes as a result of health treatments, the focus can be placed on the mechanical changes of tissues and cells. As discussed in a recent article of Donald Ingber, the changes of mechanics and tissue structures has a big influence on the causes of different types of illness[4]. By combining these mechanical changes with the biological functions, structures and physiological behaviors, some diseases and/or treatments can be understood in a better way. A few examples where the mechanical changes of cells are used as a biomarker are listed below, giving an indication of the possibilities and importance of this way of indication.

- Malaria infection. As a result of deposited proteins of the plasmodium falciparum parasite, the membrane and the cytoskeleton of red blood cells will change within three stages, namely a ring-state, a trophoziot state and a schizont stage[5]. Based on stress-strain cell experiments clear mechanical differences were found between these parasitic stages where a deformability decrease of the cell was observed[5].

- Circulating tumor cell (CTC). Tumor cells can leave the primary tumor and move through the blood or lymph vessels, from that moment the tumor cells are called CTCs. The CTC can start a new tumor at another location within the body (metastasis). A change in mechanical properties was observed during the transformation from a normal cell to a tumor cell, namely a decrease in stiffness and as a result of this an increase of deformability[6].

- Atherosclerosis. Monocytes will enter the arteries through damaged endothelial cells and change to an activated cell state. In combination with low-density lipoproteins which are oxidized, the activated monocytes will change in macropharges and finally

to foam cells. A fatty streak will be created within the arteries as a result of these foam cells, the fatty streak will grow and results finally in a blood vessel constriction or a total blockage[7]. Monocytes are involved within each step of the atherosclerosis development and the cytoskeleton will change within each step to move for example through barriers. The obtained stiffness and the deformability of the monocyte changes are specific for the different atherosclerosis development stages[7].

2.2 Microsystems and cell measurement methods

To realize *in vitro* measurements on for example cells or tissues, the research area of microsystems gives a lot of possibilities and opportunities to perform and develop specific process steps and/or total measurement devices. Within microsystems fluid flows, mixing and separation processes, actuations, heat processes, etc. can be performed on a micrometer length scale. The possibility to create structures at very small scales (even smaller compared to cell diameters) and the possibility to control fluid flows with small volumes in an accurate way makes this type of systems ideal for cell characterizations. Because of these advantages different subdomains are developed within the microsystems research direction like lab-on-a-chip devices where multiple laboratory functions are realized on a chip format, organs-on-a-chip to mimic *in vivo* processes of the human body, biomedical microelectromechanical systems and micro total analysis systems[8]. Also for cell characterizations already multiple measurement methods have been developed and are being used, each with their advantages and disadvantages. Some methods are designed for surface measurements, others for a part of the cell, for a total cell measurement or for the measurement of a group of cells. Below a few measurement methods are listed which are based on measurements on a total cell or a group of cells to get an idea of the available principles. This list of methods is just a small selection, for a wider overview of measurement methods the thesis of A. Ravetto[9] is recommended.

- Compression by a membrane. An example of a microfluidic compression method on cells is given in figure 2.1, subfigure A. A group of cells is collected within a flow channel which is separated from a control channel by a polydimethylsiloxane membrane. By adding a higher pressure on the control channel the membrane will deform into the flow channel. When the pressure in the control channel is high enough the membrane will touch the cells in the flow channel and by an increasing pressure the compression force and in this way the deformation on the cells will increase. With the use of a microscope and camera the cell deformation can be recorded and coupled to the applied pressure during the analysis phase[10].

- Constriction channels. The use of a constriction channel which has a smaller width compared to the cell diameter can be used to deform a cell. With the use of a pressure induced control at the inlet side, the cells and fluid will flow and the cells will enter the constriction channel. Within this constriction channel the traveling time over the constriction channel length can be measured, which gives in combination with the undeformed cell diameter, an indication of the cell stiffness. No real cell parameters can be determined with the use of this method, but only results which are measured with this specific method itself can be compared with each other. The traveling time can be determined with the use of image analysis of a video or with the use of an electric circuit as is illustrated in figure 2.1 at subfigure B[11].

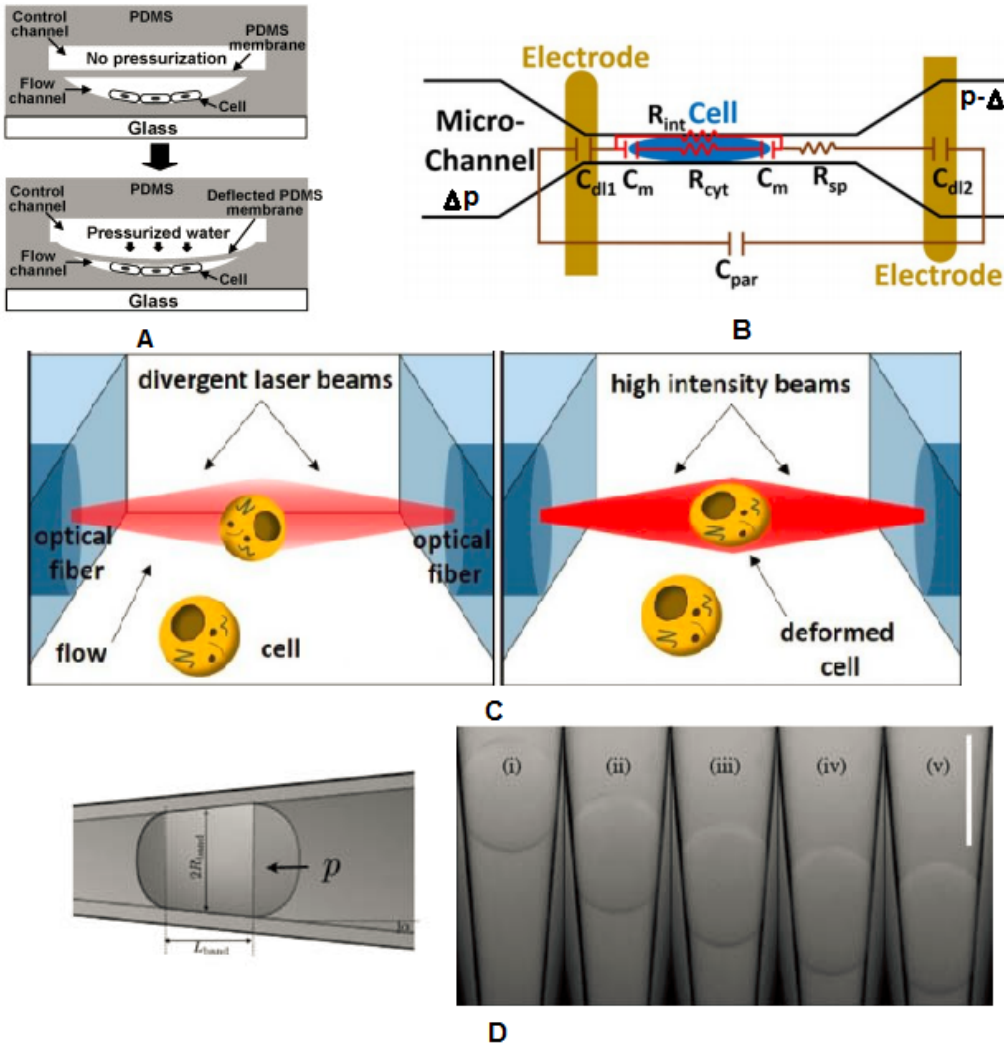

Figure 2.1: *Measurement method examples for mechanical property determination of cells. A: cell compression by an activation channel and a deformable membrane*[10]*. B: cell deformation and traveling time determination of cells through a narrow constriction channel* [11]*. C: cell deformation with the use of laser intensities to realize an optical trap, with left the undeformed and right the deformed situation*[12]*. D: capillary micromechanics method where cells are compressed by an external pressure and deform into a tapered capillary tip to determine the shear and the compression modulus. Left the schematic principle and right a particle deformation as a result of the applied external pressure*[13]*.*

- Optical stretcher. Cells flow through a microfluidic channel where at specific locations cells where trapped with the use of low intensity laserbeams which are arranged oppisite to each other. As a result of the two divergent laser beams a gradient force on the cell acts in the direction towards the center of the optical trap. By increasing the laser intensities, the cell will deform because of the resulting optical surface forces as can be seen in figure 2.1, subfigure C[12]. An advantage of this method is that it is a non-contact measurement method, where for example friction and wall forces do not play a role during the measurement.

- Capillary micromechanics. A cell or particle is captured within a tapered capillary tip and deformed within the tip by the stepwise increase of an external pressure. With

the use of image analysis, parameters like the the volume change and the strain values in specific directions can be calculated, and finally the shear and compression modulus can be determined. A schematic representation of the measurement principle and an example of a particle deformation as a result of an applied pressure are given in figure 2.1[13], subfigure D.

Based on the different measurement types, of which only a selection is discussed above, the preference within this investigation is to use a single cell measurement method. Specifically, the capillary micromechanics method because of the opportunities, materials and knowledge at the TU/e . This method has the specific advantage that the results are quantitative. The method will be explained in more detail in section 3.2.

2.3 Cell components related to mechanical properties

In the previous subsections the importance of cell mechanics and ways how to measure these were explained. Important is to know how these mechanical properties vary between different cells or cell stages. In general, the mechanical properties of cells depend on a number of conditions, namely the the time scale for performing the measurement, the degree of deformation applied to the cell, the direction of the pressure or force on the cell, and the physical location of the cell (environment)[14]. Another given fact is that a cell consists of multiple components which are located within the cell, resulting in an inhomogeneous distribution of material[14]. Some cells exhibit a stress stiffening behavior because of the cytoskeleton, leading to a nonlinear elastic behavior[15].

The cytoskeleton is the main component within each cell related to cell division and motility, and which determines the shape and the internal organization. It thus has a big influence on the total mechanical behavior[16]. The cytoskeleton is composed of three main collaborating types of elements, which are the microtubules, actin filaments and intermediate filaments, which all have a difference in element size and protein composition[16]. The microtubules grow from the centrosome of a cell (mostly located against the nucleus and thus more cell center oriented) in the directions of the cell membrane. This component is responsible for the orientation of cell organelles, for the resistance against compression forces and, because of its hollow structure, for the transport of genetic material[17]. The actin filaments are mostly located at the plasma membrane and one of the functions is to endure larger tensions[18]. Actin consists of two types where globular actin (G-actin) is the protein state after production within the cell and filamentous actin (F-actin) is the state where multiple molecules have created a helix shaped chain[18]. The intermediate filaments have an oblong shape, are less dynamic and have a main function to support the microtubular components[16]. An overview and representation of the cytoskeleton components can be seen in figure 2.2[19].

There are multiple mechanical stimulations which can be applied to cells to measure the response, for example uniaxial and biaxial tension, shear, compression, bending, hydrostatic pressure and twisting[10] which have all their own effect on a specific cell type. At a certain amount of deformation not only the cytoskeleton environment will be measured, but also the nucleus will be deformed and play a role related to the measured mechanical properties.

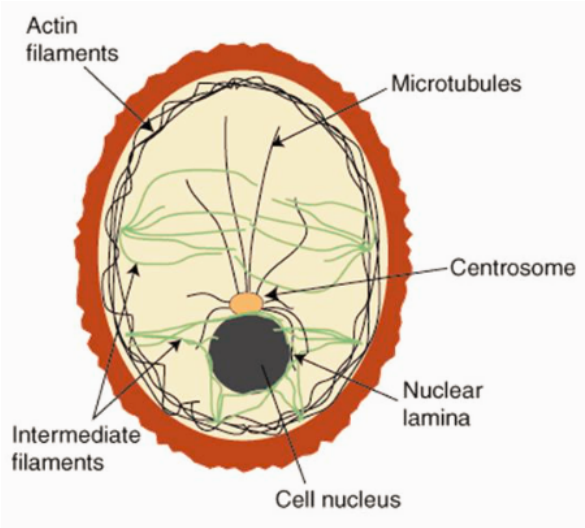

Figure 2.2: *Cytoskeleton. Different cytoskeleton components and orientations within a cell*[19]

2.4 Research goal and report part sections

As described in the review of J.F. Sleeboom et al.[20] secondary tumors play a major role in the total amount of cancer deaths and are the result of the metastasis process. During the metastasis process, tumor cells cross multiple times vessel walls and migrates through tissues to move through the blood vessels to the later on secondary tumor location. This cancer metastasis process contains of multiple steps which are dependent on cell characteristics as well as on the microenvironment of the tumor[20]. One of these microenvironment elements is the fibrous extracellular matrix through which the cell moves during the invasion phase[21]. In the investigation of H. Eslami Amirabadi et al.[21] a method has been developed to investigate the invasion behavior which uses polycaprolactone matrices with different gap sizes between two microfluidic channels to mimic the extracellular matrix. The MDA-MB-231, CAMA-1 and MCF-7 breast cancer cell lines were cultured inside the devices, they migrated through the matrix with the use of a chemical stimulus, and the invasion depth was determined after three days[22]. Differences in invasion depth were found between the cells and to understand the difference in invasion of the different cell types in a better way, the mechanical properties of single cells of these cell types must be determined and compared.

The main goal of this research is to determine the mechanical properties of the MDA-MB-231 and MCF-7 breast cancer cell lines with the use of the capillary micromechanics method. Knowledge on the mechanical properties of specific cell types can also be used to understand cell behaviors under specific circumstances in a better. However, when the mechanical properties of a cell type are known, they can be used for the validation of other new cell measurement systems.

In the next chapters of this report the MDA-MB-231 and MCF-7 cell lines are described as well as their culture protocol, with the main focus on the MDA-MB-231 cells. The capillary micromechanics method is briefly explained, as well as the theory on which the experimental analysis is based. The device fabrication and preparation steps are given. A cell morphology and viability experiment is described followed by an elasticity and time-dependency experiment. In chapter 4, first the results of the cell line behaviors under normal circumstances are described, results of the side-experimenents are given next, and the shear and compression modulus values are finally displayed and compared. All results are discussed

in chapter 5 and the behavior of both used cell lines is compared and evaluated against literature. Finally a conclusion is given in chapter 6, followed by recommendations for a further investigation in chapter 7.

3 Materials and methods

In this chapter, first the used cell types are introduced as well as their culture protocols. The principle of the capillary micromechanics method is discussed briefly and in combination with the theoretical analysis. A protocol is given of how to fabricate and prepare the devices for an experiment followed by a first morphology and viability experiment description for the MDA-MB-231 cell line. Finally, the capillary micromechanics method is described in a more experimental way, an elasticity and time-dependency experiment are described and the principle of the data analysis is given followed by an error analysis.

3.1 Cell lines

In this investigation two breast cancer cell lines were used, namely MDA-MB-231 and MCF-7. Both cell lines were kindly given by Dr. John W.M. Martens from the Erasmus Medical Center in the Netherlands. The cells have both an adherent way of culturing, where the cells spread and grow over the surface area instead of a free-floating way within the total culture medium. As described in a document of the European Collection of Authenticated Cell Cultures (ECACC) the MDA-MB-231 cell line is an "*epithelial, human breast cancer cell line which was established from a pleural effusion of a 51 year old woman*" [23]. The MCF-7 cell line has an epithelial-like morphology and is obtained by a pleural effusion from a 69 year old woman[24]. Both breast cancer cell lines are characterized based on the estrogen receptor (ER), the progesterone receptor (PR) and the human epithelial receptor 2 (HER2), with MDA-MB-231 (ER-, PR- and HER2-) and MCF7 (ER+, PR+ and HER2-)[25]. In this section the culture steps are described for both cell types, which must be used to prepare the cells for experiments and for cell passaging.

3.1.1 Cell passaging

Both cell types were cultured in RPMI-1640 Glutamax medium (Thermofisher Scientific, Gibco) [26] in combination with 1% (v/v) Penicillin/Streptomycin (Lonza) and 10% (v/v) Foetal Bovine Serum (Bovogen Biologicals). For a cell passage the old medium from the growth flask was removed and the flask was rinsed two times with Phosphate Buffered Saline (PBS) EDTA (BioWhittaker, Lonza), which is a salt solution with a pH of 7,5. Trypsin EDTA (Lonza) was thawed within a water bath of 37°C and added within the flask, where an amount of 1 mL for a T25 flask and 2 mL for a T75 flask was used. Trypsin is an enzyme which breaks down the proteins which are used by the cell to adhere to the growth surface. The flask was placed for 4 - 4,5 min in a humidified incubator with the following conditions: 37°C, 5% CO_2 and a humidity around 90%. 5 mL of new medium was added to the flask to stop the effect of the trypsin on the cells and to prevent a further breakdown of proteins and corresponding cell damage. The solution from the flask consisting of trypsin and culture medium was placed into a 15 mL polypropylene test tube with screw cap with the use of a pipette. The flask was flushed with 1-2 mL of medium to collect the remaining cells. The tube was placed in the Mega Star 1.6 centrifuge with a 3655 bucket. A counterweight with the same amount of liquid was placed at its mirror position and the following settings were used to centrifuge the cells: ω = 900 rpm, t = 5 min and the acceleration and decelleration were 9 m/s^2. After the centrifugating step the cells were concentrated at the bottom of the tube, the medium-trypsin solution located on top of the cells was removed with the use of a pipette and 1 mL of new medium was added to the cell pellet. Cells were counted with

the use of the nucleocounter NC 200 in combination with a VIA1-cassette (Chemometec) to determine the concentration of cells per milliliter, the average diameter in micrometers and the viability percentage, when needed for an experiment. For a cell passage to another flask the desired ratio of cells was chosen related to the flask surface area and the chosen amount was placed within 5 mL of new medium for a T25 flask and 13 mL of new medium for a T75 flask.

3.1.2 Cell growth rate and morphology

Both cell lines were investigated under normal cicumstances. These normal circumstances are defined here as the optimal conditions within an incubator, in medium with additives, and without external factors like an applied pressure. With the use of a Cytomate imaging system the images were produced with 30 minute time steps for four till five days within an incubator while cells were in culture. These images were used to determine the growth rate of both cell lines. With the EVOS imaging system (appendix 8 table 8.3) images were made of cells after one day to look at the cell morphologies of both cell lines in an adherent state.

3.2 Capillary micromechanics method

In this subsection, the capillary micromechanics method will be described in short, followed by the theoretical background and definitions which are used to calculate the mechanical properties of the measured cells.

3.2.1 Schematic measurement principle

The schematic setup of the capillary micromechanics measurement method is given in figure 3.1[27]. This setup consists of a tapered glass capillary which is connected with a tube to a pressure regulation element. The pressure regulation can be realized using a height change of a fluid container based on gravitational forces, or by using a pressure driven regulation system. As can be seen in this figure, the capillary is placed within a fluid container to circumvent the occurence of surface tension forces at the tip location.

A cell must be captured within the tapered region of the capillary and when a cell is just touching the capillary tip walls without further movement, the pressure at both sides of the cell in the longitudinal direction of the capillary is equal. This cell position results in a stationary point at an imposed pressure difference of zero. Starting from this pressure state, the pressure is increased in small steps with a waiting time after each step to obtain a new stationary position. The increase of pressure deforms the cell more and more and images are made for each applied pressure. All the images together from a single cell measurement; they can be used to perform an image analysis, from which both the shear modulus G Pa and the compression modulus K Pa can be determined. The compression modulus represents the resistance of a cell to a change in volume and the shear modulus represents the resistance of a cell to a change in shape[28]. With this method a single cell measurement can be perfomed where the assumptions are made that the measured particle or cell has an elastic behavior, that the tapered region of the capillary is straight, that the friction between the cell and the capillary wall is equal to zero, and that the cell has the same properties in all directions (isotropic behavior).

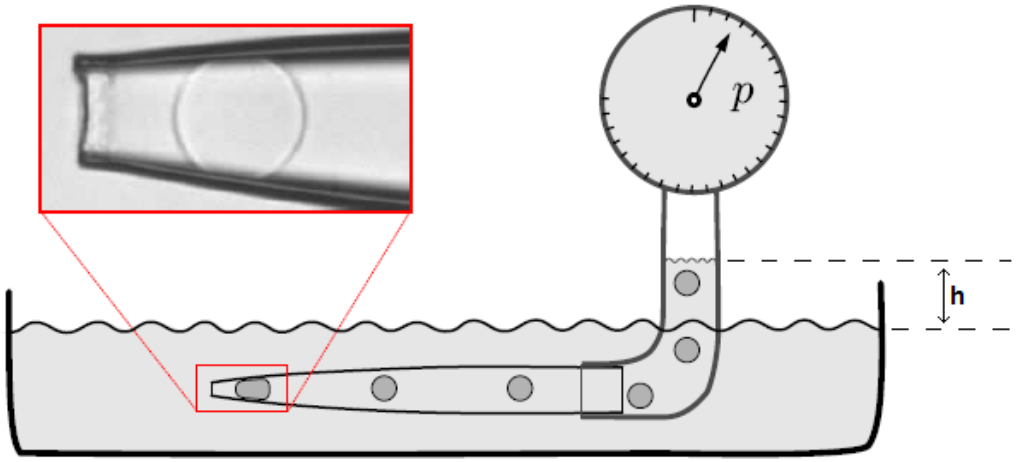

Figure 3.1: *Schematic setup for the capillary micromechanics method*[27]*. Pressure adjustable part which is connected to a tapered glass capillary with tubes. A larger pressure results in a larger deformation of the cell, which can be used for determining the compression and shear modulus of the cell. h is the height related to the pressure adjusted with gravitational forces.*

3.2.2 Theoretical background

The external pressure obtained because of an applied liquid height can be calculated with equation 3.1, with h m the height, g $\frac{m}{s^2}$ the gravitational acceleration, ρ $\frac{kg}{m^3}$ the density of the fluid and $P_{external}$ Pa the external pressure. With $g = 9{,}81$ $\frac{m}{s^2}$ and the assumption that PBS has the same density as water (1000 $\frac{kg}{m3}$) a pressure change of 10 Pa is the result for each millimeter of height change. The force acting on the cell as a result of this pressure can be calculated with equation 3.2[28] with R_{back} the radius at the pressurizing side (figure 3.2) and A_{back} the area of the cell where the cell is in contact with the capillary wall at the pressurizing side. With the assumption that there is no static friction, the external applied force must be equal to the wall force in the longitudinal direction for each stationary situation. The relation between the wall force and the external force can be seen in equation 3.3, with α the angle between the bottom or top wall of the tip and the longitudinal direction of the capillary (figure 3.2). The wall pressure can be determined by dividing the wall force by the contact area, $A_{contact}$, between the cell and the capillary wall as is given in equation 3.4. Here L_{band} is the length measured along the middle between the back and the front contact points and R_{front} is the radius at the front where the cell is in contact with the capillary wall at the tip side (figure 3.2).

$$P_{external} = \rho g h \tag{3.1}$$

$$F_{external} = p_{external} A_{back} = p_{external} \pi R_{back}^2 \tag{3.2}$$

$$F_{wall} = \frac{F_{wall,longitudinal}}{\sin(\alpha)} = \frac{F_{external}}{\sin(\alpha)} \tag{3.3}$$

$$P_{wall} = \frac{F_{wall}}{A_{contact}} = \frac{F_{wall}}{\pi(R_{back} + R_{front})\sqrt{(R_{front} - R_{back})^2 + L_{band}^2}} \tag{3.4}$$

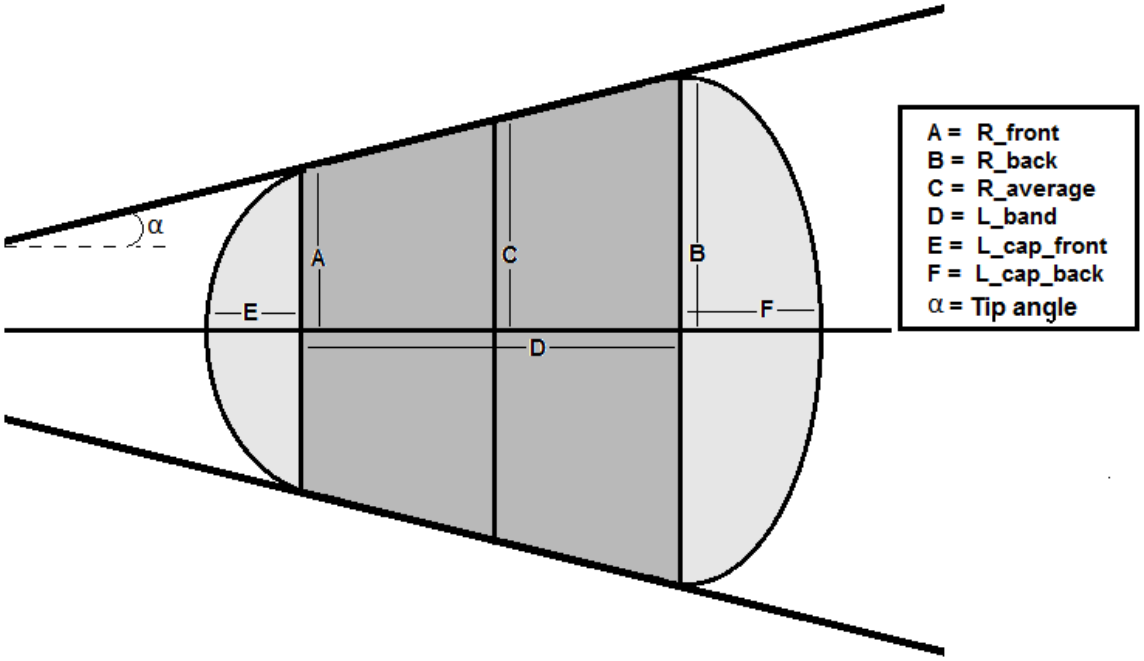

Figure 3.2: *Lenght and shape definitions of a cell captured in a tapered capillary. Multiple radius and length values are given and the cell shape is divided into two spherical caps and a cone frustum.*

The assumption is made that no plastic deformation of the cell will take place and that the cell behavior can be described with a linear elastic model[28]. At a stationary position of the cell, where no further cell movement occurs, the internal and external stresses are equal to each other. The stresses in the longitudinal (z-direction) and the radial direction (r-direction) can be described as a function of the shear modulus, the compression modulus and the strains in these two directions (ϵ_r and ϵ_z). The equations to describe these stresses are given with equation 3.5 and 3.6 for an isotropic material[27]. When these equations are solved with the wall pressure equal to the stress in the radial direction and the pressure because of the height change equal to the stress in the longitudinal direction, equations 3.7 and 3.8 are the result for the compression modulus and the shear modulus respectively [27]. In equation 3.7 the numerator represents the average force on the cell from all directions and the denominator the volumetric strain, where $2\epsilon_r + \epsilon_z$ is the summation of strains in all cartesian axis directions and can be given as the volumetric strain, ϵ_V. In equation 3.8 the numerator represents the average difference between the wall pressure and the external applied pressure and the denominator represents the strain difference between the radial and longitudinal directions.

$$\sigma_r = K(2\epsilon_r + \epsilon_z) + \frac{2}{3}G(\epsilon_r - \epsilon_z) \tag{3.5}$$

$$\sigma_z = K(2\epsilon_r + \epsilon_z) - \frac{4}{3}G(\epsilon_r - \epsilon_z) \tag{3.6}$$

$$K = \frac{(2P_{wall} + P_{external})/3}{2\epsilon_r + \epsilon_z} = \frac{(2P_{wall} + P_{external})/3}{\epsilon_V} \tag{3.7}$$

$$G = \frac{(P_{wall} - P_{external})/2}{\epsilon_r - \epsilon_z} \tag{3.8}$$

The strain values in the radial and the longitudinal directions can be determined with equations 3.9 and 3.10 for each deformed cell state. In these equations $L_{band,0}$ and $R_{average,0}$ are the values at the zero pressure state which is defined as the state where the cell is undeformed and L_{band} and $R_{average}$ are the same dimensions but then at each deformed situation (figure 3.2 for an example of a deformed cell state). The $L_{band,0}$ and $R_{average,0}$ lengths for the undeformed state can be determined based on image analysis on the single image related to the undeformed cell state and L_{band} and $R_{average}$ values are based on image analysis on each image related to a deformed cell state. The volume at the zero pressure state V_0 and the volume at deformed state V are determined by splitting up the cell shape into three subshapes (different grey colors in figure 3.2) and by adding up the three subvolumes. V_0 is determined based on image analysis on the first image related to the undeformed cell state with equation 3.11 and V on image analysis on each image related to the deformed cell states with equation 3.11. The subshapes of the volume are a spherical cap with R_{front} for the base radius and $L_{cap,front}$ for the height, a second spherical cap with R_{back} the base radius and $L_{cap,back}$ for the height, and a conical frustum subshape in between the two spherical caps. The total volume calculation is given in equation 3.11. The volumetric strain is calculated with equation 3.12. The shear modulus is determined by the slope of the fit through the points with $(P_{wall} - P_{external})/2$ against $\epsilon_r - \epsilon_z$[9]. The compression modulus is determined by the slope of the fit through the points with $(2P_{wall} + P_{external})/3$ against $\frac{\Delta V}{V}$[9], where $\frac{\Delta V}{V}$ is the volumetric strain, another representation of the denominator in equation 3.7.

$$\epsilon_r = \frac{R_{band,0} - R_{band}}{R_{band,0}} \tag{3.9}$$

$$\epsilon_z = \frac{L_{band,0} - L_{band}}{L_{band,0}} \tag{3.10}$$

$$\begin{aligned} V = V_{front,cap} + V_{cone} + V_{back,cap} = \tfrac{\pi L_{cap,front}}{6}(3R_{front}^2 + L_{cap,front}^2) \\ + \tfrac{1}{3}\pi L_{band}(R_{front}^2 + R_{back}^2 + (R_{front}R_{back})) + \tfrac{\pi L_{cap,back}}{6}(3R_{back}^2 + L_{cap,back}^2) \end{aligned} \tag{3.11}$$

$$\epsilon_V = \frac{\Delta V}{V_0} = \frac{V_0 - V}{V_0} \tag{3.12}$$

With the use of K Pa and G Pa other material parameters can be determined like the Young's modulus E Pa given in equation 3.13 and the Poisson ratio ν given in equation 3.14[29].

$$E = \frac{9KG}{3K + G} \tag{3.13}$$

$$\nu = \frac{3K - 2G}{6K + 2G} \tag{3.14}$$

3.3 Microcapillary devices

To perform the capillary micromechanics method, devices were fabricated and with specific steps prepared for an experiment, as will be described in this subsection.

3.3.1 Device fabrication

An example of a device is given in figure 3.3, with left a top view and right a side view. The tapered glass capillaries were made with the use of the micropipette puller P-97 from Sutter Instruments Co. (Appendix 8 table 8.1). The goal for each capillary was to create a short taper to minimize the amount of contact of a cell with the glass walls and in this way to minimize the effect of the wall friction. The final focus was to create tip diameters of 7 μm ($\pm$ 2 μm), which were small enough to realize a stepwise deformation of the cell and big enough to avoid fast clogging because of cells and dirt and to avoid cell rupture. For the capillaries, 1B100-4 glass tubings (World Precision Instruments) with an inner diameter of 0,58 mm, an outer diameter of 1 mm and a length of 100 mm[30] were used to create two tapered capillaries at a time. To create tips within the range of interest the following micropipette puller settings were determined within the possible device ranges: heat = 620, pull = 0, velocity = 13, time = 150 and pressure = 500. The combination of the used type of glass tubings and the heating fillament characteristics results in a specific amount of heat which is needed to melt the glass. With the use of a ramp-test, the heating value can be determined to melt the glass which resulted into a heat value of 550 for the glass tubes described above and the installed heating fillament. When the heating fillament is replaced because of damage in combination with the device settings given above, other tip angles and diameters may be the result. With the difference between the measured ramp test value (550) and the used heat to create the final tapered capillary (620) a value is the result which can be used in combination with a ramp-test value of the new heating fillament to determine the new heating value for the capillary production which is close to the original settings described above. With the determined settings still a variability in diameters was the result, so the tip diameters that were too small were further processed with the use of the MicroForge MF-900 (appendix 8 table 8.2). For all produced capillaries the tip diameter was measured with the Olympus BX51 brightfield microscope (Appendix 8 table 8.4) with a 50x objective lens in combination with a digital measurement function and only the tip diameters of 7 μm ($\pm$ 2 μm) were used for the devices. A device consists of a microscopic slide (VWR) with a thickness of 1 mm as a base surface which makes it possible to fit the final device in almost all microscopes and microscope holders. On top of this base surface, the capillary was glued sticking out a few millimeters compared to the microscopic slide to make it possible to connect the tubing to the glass capillary. Around the capillary tip a fluid reservoir consisting of a slice of a syringe was connected to the glass slide, which can be filled with PBS to compensate for the surface tension at the tip location of the capillary. The larger size of the reservoir was to ensure visualizing as much as possible of the capillary to be able to intercept cells and air bubbles in time.

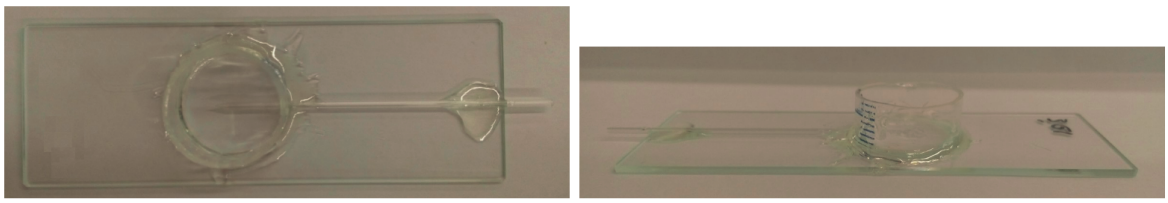

Figure 3.3: *Microcapillary device. Left: top view. Right: side view. Tapered glass capillary with desired tip diameter glued to a microscopic slide with a fluid reservoir around the tip location.*

3.3.2 Device preparation

Before a device was ready to use for an experiment three preparation steps were needed as illustrated in figure 3.4 which were performed with the use of the EVOS imaging system. First, Bovine Serum Albumin (BSA) was entered into the fluid reservoir and withdrawn from the tip to the inlet with the use of a syringe to coat the glass capillary. This coating step was needed to minimize the friction force between the cells and the glass walls. The BSA is a protein which blocks bindings which are non-specific related to the cell membrane because of the presence of molecules which are non adhesive[31]. The BSA powder (fraction V, Roche Diagnostics GmbH) was dissolved in PBS to create a 1% (w/v) solution which was two times filtered with a 0,2 μm filter before usage to remove larger particles. After approximately five minutes of coating the BSA was removed from the reservoir. In the second step the same principle was repeated with PBS to flush the capillary and to remove the BSA remains. After removing the PBS from the reservoir, air was drawn through the capillary to dry the inside as given in step number three. The reason for withdrawing the fluids and air instead of injection was to minimize the chance of tip clogging because of possible dirt present in the capillary or used tubings.

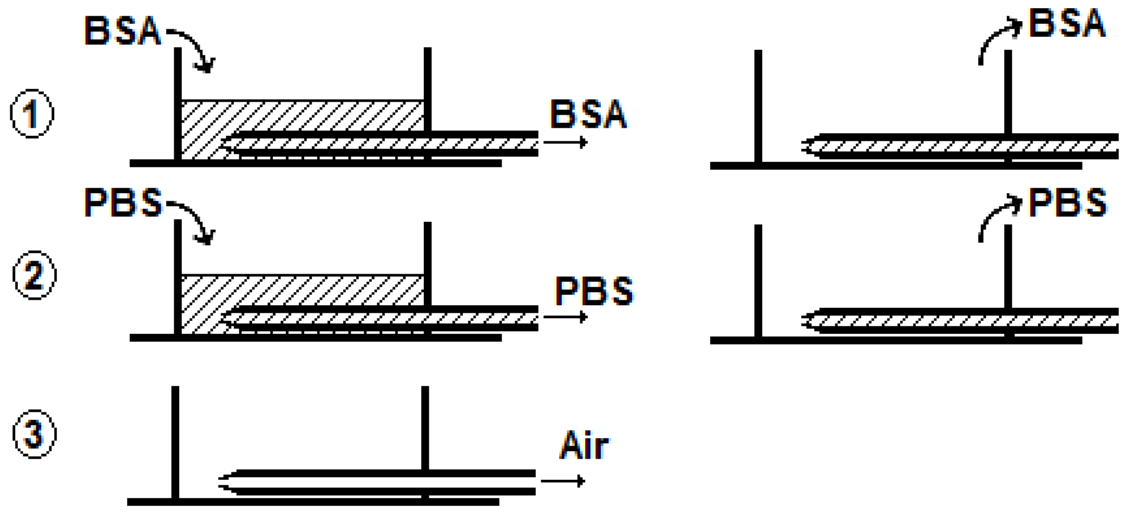

Figure 3.4: *Microcapillary device preparation steps. 1: BSA coating, 2: PBS flush and 3: dry.*

3.4 Cell morphology and viability

During the capillary micromechanics experiment, cells were used in combination with PBS, medium with additives and the BSA solution. Within this subsection an experimental procedure will be described to investigate the cell morphology and cell viability of the MDA-MB-231 cells in these solutions at room temperature. Only this cell type was used for this experiment with the goal to create a functional experimental setup which can be used for all final measurements related to the usage of the solutions. When the effects of these solutions are known they can be used to exclude atypical cell behaviors as a result of the use of these solutions during the microcapillary experiments.

Four situations in combination with cells were investigated as listed below:

1. Medium with additives in uncoated well.

2. PBS in uncoated well.
3. Medium with additives in coated well.
4. PBS in coated well.

To have the same cell treatments and history of the cells during alle experiments a T75 flask with a high confluence value was divided over four T25 flasks, were two flasks were used at the day with the uncoated experiment and the other two at the second day for the coated experiment. In this way for each individual experiment a new T25 flask was used and cells could be used immediately after suspending the cell pellet within 1 mL of medium or PBS dependent on the situation which was investigated at that time.

For the uncoated situation in combination with medium, the cell pellet was mixed with 1 mL of culture medium and the average diameter, the viability percentage and the amount of cells per milliliter was measured with the use of a VIA1 cassette in the nucleocounter. Three uncoated wells of a 6-well plate with a surface area of 9,5 cm^2 were filled with 3 mL of medium and in each well 300 μL of the cell solution was added and mixed with the use of a pipette. To get information about the cell morphology immediately after this start situation (t=0) four pictures were made of each well with the use of the EVOS microscope at a 20x magnification. The well plate was placed outside the incubator and after each ten minutes the total well plate was shaken slowly to avoid cell attachement to the bottom surface of the wells. After 60 minutes again four pictures were made of each well to get information of the morphology. After making the pictures, the cell solution was placed within a tube for each well and another milliliter of medium was used to collect the remaining cells from the well surface. Each tube was centrifuged (900 rpm for 5 min) and the cells were again placed in 1 mL of medium. A non-diluted amount of 300 μL of cell solution was used from each well for obtaining viability information with the use of the VIA1 cassette. The same principle was repeated at the same day with a new T25 flask were all the medium steps were replaced by PBS (situation 2). The other two T25 flasks were used for the experiment with coated wells one day later (situations 3 and 4). 1 mL of 1 % BSA solution was placed in each well for 10 minutes and after this time the BSA was removed and each well was flushed with 1 mL of PBS to remove the remaining BSA. Again the same experimental protocol was used as the uncoated situation to obtain the viability information and the morphology images. Because of the higher concentration of cells because of the extra cell growth day, an amount of 200 μL of cell solution was placed within each well to avoid bigger groups of cells, to make the final analysis on single cells more easily and to distribute an equal amount of cells compared to the other measurements.

With the use of the "imdistline" function of the Matlab program it was possible to count the amount of pixels within the images over a specific distance. First, the length of the 200 μm distance bar was measured in pixels as illustrated in figure 3.5 A.

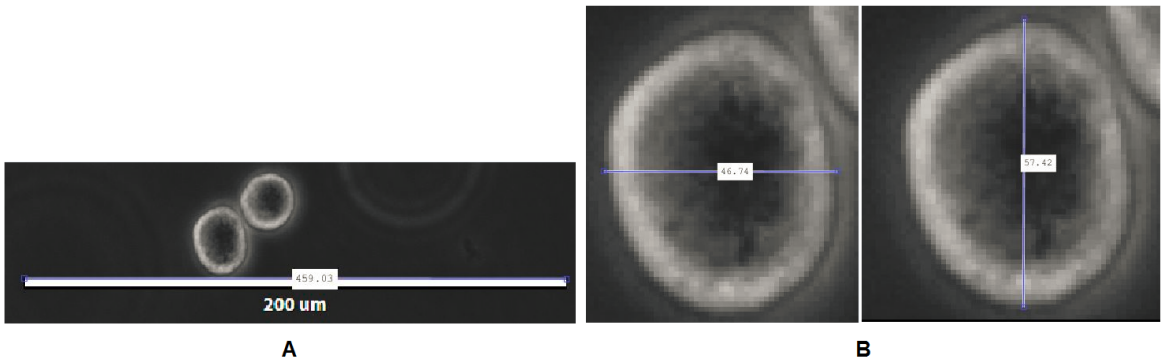

Figure 3.5: *Pixel counting with "imdistline" Matlab function. A: pixels related to 200 [µm] distance bar. B: left horizontal cell measurement and right vertical cell measurement.*

For each medium or PBS, coated or uncoated and start or end situation, two pictures were used from each well, with for each picture four cells which were measured in both the horizontal and the vertical direction as can be seen in figure 3.5 B. In this way different locations, the orientation of the cells and the different wells were taken into account for an estimation of the cell diameters in the different situations. With the use of the VIA1-cassette values and the obtained images of the EVOS microscope, an analysis was done of the morphology and the viability of the cells.

3.5 Capillary micromechanics measurement setup and protocol

The principle of the capillary micromechanics measurement method is described in subsection 3.2 and the device fabrication and treatment in subsection 3.3. In this section the measurement setup and the protocol are described in more detail. Information related to the build up phase of the experimental setup and related to the experimental protocol can be seen in appendix 12.

3.5.1 Measurement setup

The Zeiss Axiovert 200M (appendix 8 table 8.5) was chosen to use because of the possibility of both fluorescence imaging and bright-field imaging options, the presence of a temperature control within an incubation box, an installed Axiocam camera and a wide variety of filters and easy to use microscopic stages.

For the pressure control a rough z-stage was chosen to approach the same level as the microscopic stage surface and for a faster height difference realization (figure 3.6). On top of this rough z-stage a fine z-stage was placed (figure 3.6) where one rotation of the level change wheel was equal to 0,5 mm change in height and where each rotation was divided into 50 smaller steps to make it possible to achieve small accurate height changes. At the fine z-stage a 90 degree angle bracket was connected in combination with a polycarbonate holder which was designed to clamp a 3 mL syringe (figure 3.6).

The polycarbonate holder was made in such a way that the input container syringe was oriented at a 45 degree angle to avoid a 90 degree buckling point within the tube, to support a better cell solution flow and to avoid cell clogging within the total circumference of the syringe. The syringe was through a dispensing tip connected to a 0,86 mm inner diameter tube and this tube was connected to one of the devices as given in subsection 3.3 as is

illustrated in figure 3.6. For every measurement the tube was placed as much as possible at the same height to avoid cell accumulation in one of the minimum height positions, and the opening where the tube enters the incubation box was made to be as small as possible to accomplish a temperature as close as possible to 37 °C.

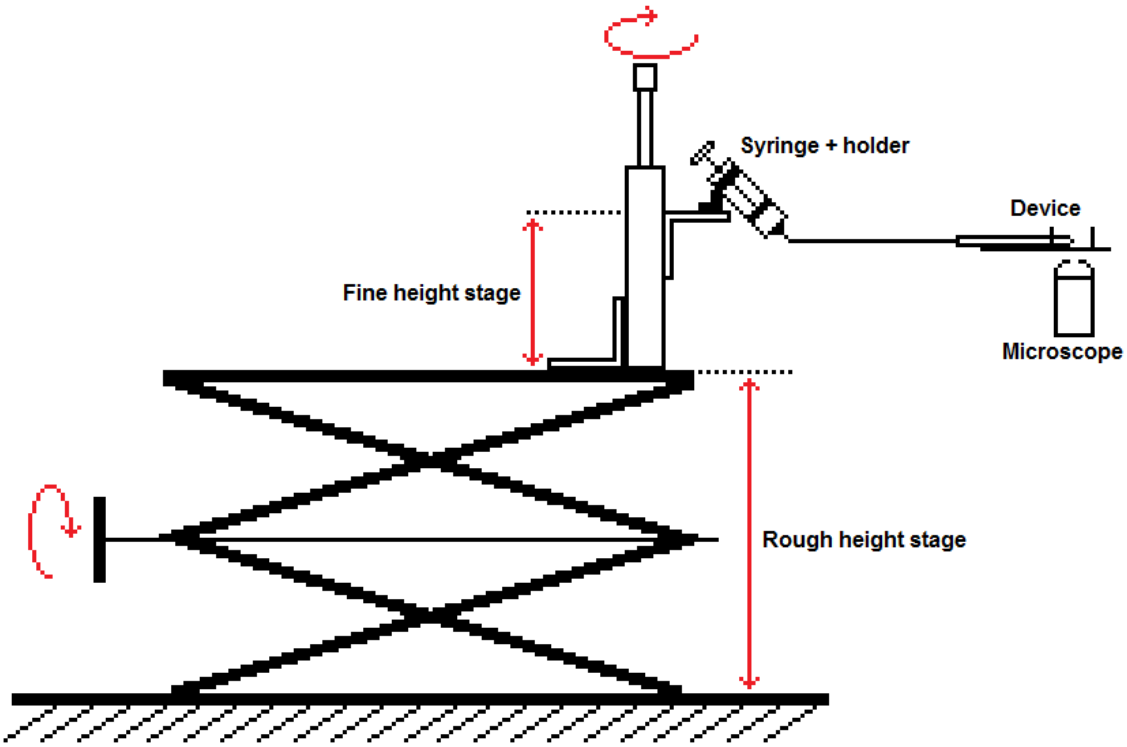

Figure 3.6: *Schematical experimental setup. Height changes by a rough and fine z-stage, 45 degree angle syringe holder with input container syringe and a by tubings connected device on top of the microscope objective.*

A 20x magnification objective was used from the company Zeiss (PH2 Plan-Neofluar 20x/0.50) which resulted in combination with a 1.6x optovar magnification changer in a final magnification of 32x. This objective has a free working distance of 2 mm which makes it suitable to use in combination with the fabricated device thickness [32].

3.5.2 Experimental protocol

Before the start of an experiment the cells from a confluent T75 flask were prepared within 3 mL of PBS. PBS was chosen to use because of the absence of additions (nutrients, antibiotics, etc.) which are present in for example the medium solution. PBS is non-toxic to cells and has properties which match the properties of the human body, namely the concentration of ions and the osmolarity[33]. Not only the devices, but also the tube and the input container syringe were coated with BSA to minimize the friction and the cell adhesion. At the start the temperature control was set at 37 °C and it took approximately ten minutes before this temperature was reached. Beside the temperature the experiments were performed without the for cells most ideal incubator conditions. The syringe plunger of the syringe at the inlet was placed halfway through and the dispensing tip and the tube were connected. The cell solution was mixed with the use of a syringe or by tapping the tube for a long time on a surface. The cell solution was withdrawn into the syringe until a small part of the syringe

was filled. By pressing the plunger a liquid bubble at the end of the tube was realized, which meant that the air at the end of the tube was removed and after that the tube was connected to the device. The device was placed in the microscopic holder and the tube at the end was connected to the x-y stage surface of the microscope with some tape. The tip of the glass capillary was placed in focus, the extra 1.6 magnification option was set and PBS was added to the tip reservoir till the fluid level was a few millimeters above the tip location. The plunger at the inlet reservoir was removed and after that the plunger was used to pressurize the system by hand to remove the air from the capillary through the tip. When the air was removed the solution with cells was immediately located in the neighborhood of the tip. The tubes were checked for present air bubbles and the air in the dispensing tip was removed by manually tapping on it. At the start the fine z-stage was positioned a bit above the lowest position and with the use of the rough z-stage the level of cell solution was placed above the level of the fluid in the fluid reservoir at the device. By moving the x and y stages of the microscope the capillary could be seen up to a few millimeters away from the tip where the fluid velocity was lower. When a cell was detected which was moving to the tip location, at first the rough z-stage was moved down to decrease the cell velocity and the cell was brought slowly to the tip with the cell being within the last part of the tip, the fine z-stage was used to decrease the cell velocity until the cell was just touching the capillary walls. When no cell was moving in the tip direction, a small pressure was applied by hand with the use of the plunger to detach the cells from the walls or from a group of cells and the same steps as described above were executed. From the moment a cell was just touching the walls the starting position of the measurement was found with an applied pressure difference of zero. A period of 1:45 min was added to create an equilibrium position for the cell and an image was made with the use of the camera on the microscope. This image was later on used for the determination of the volume, length and radius values from figure 3.2 at the undeformed state with a zero pressure difference. The height was increased with the small z-stage, with steps between one fifth till half of a rotation, being equal to 0,1 - 0,25 mm dependent on the situation, and after each step this waiting time (1:45 min) was again executed and an image was made. These steps were repeated until the cell was deformed in the capillary tip, with a maximum deformation which was allowed to add where the cell was just not touching the edge of the tip. During most measurements a small tap step was added on the base glass of the device after each new height set with the use of a piece of plastic. With this tap step a small vibration was created in the capillary with the goal to detach the cell from the walls when a cell was adhering to it (extra prevention besides the BSA coating) and to overcome a distortion of deformation as a result of friction forces. After each measurement, the cell was removed by pressurization by hand and another cell was caught within the tip.

3.6 Elasticity and time-dependency

In the capillary micromechanics analysis method the assumption is made that the cells have an elastic behavior, as previously mentioned. To investigate if this is a plausible assumption a hysteresis experiment was done with the MDA-MB-231 cell line. The same protocol was used as described in subsection 3.5.2 to increase the pressure with small steps but instead of removing the cell at the final pressure state, the pressure was decreased with the same steps until the cell was moving back into the capillary without touching the walls anymore. It was possible to investigate if the cell was moving back to its position when the pressure difference was back at zero making it possible to determine if the cell had deformed plastically. A second experiment was done to investigate the time dependent behavior of a cell within the capillary tip under pressurized circumstances. Also for this experiment the external pressure on the

cell was increased with small steps to realize a gradual deformation of the cell. At a certain pressure the cell was not pressurized any further, but held at the pressurized state while each five minutes an image was made. With this experiment the time dependent behavior of the cell was investigated while no experimental changes were applied.

3.7 Data analysis

In this section the data analysis is described, used to determine the shear and the compression modulus based on the experimentally obtained images. During an experiment images were generated for each used external applied pressure. First each image was cropped in such a way that only the information rich image parts were left in the image, which are the glass capillary tip and the catched cell. Each image from a single cell measurement was cropped in the same way, i.e. with the same amount of remaining pixels in both image directions. In the next step the set of images was loaded in the program ImageJ in combination with the pointpicker plugin. With this program seven points were selected manually, where the same amount of pixels within each image made it possible to do this selection with the same accuracy for each image. The seven points were selected in the same order for each image as illustrated in figure 3.7.

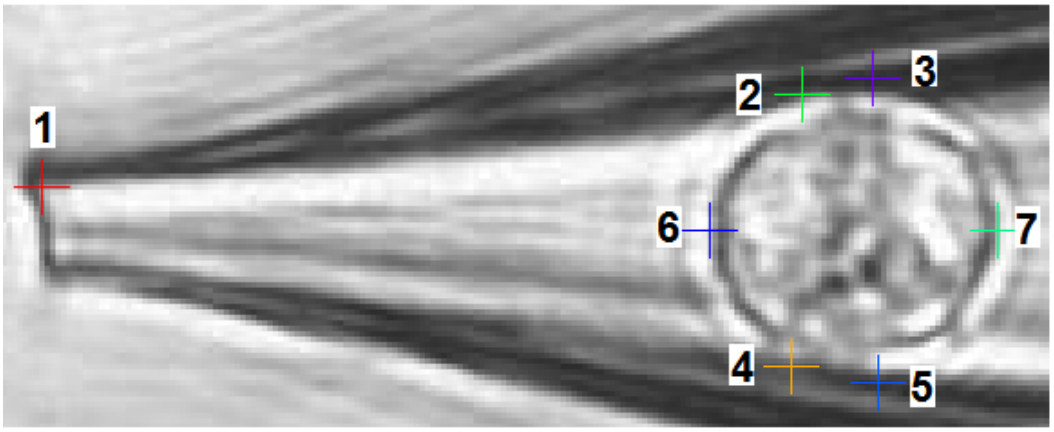

Figure 3.7: *Manually selected point locations and order for each image. Reference point (1), two extreme points between the cell and the top wall (2 and 3), two extreme points between the cell and the bottom wall (4 and 5) and the minimum and maximum spot of the cell in the longitudinal direction (6 and 7).*

These points are a reference point which must be the same for each image (point 1), two extreme points between the cell and the top wall (points 2 and 3), two extreme points between the cell and the bottom wall (points 4 and 5) and the minimum and maximum spot of the cell in the longitudinal direction (points 6 and 7). All these points together were saved in a text file containing the point number for each image, the x and y pixel number for each point, the image number and a color and ID value for each point. A second text file was made containing the image number and the height value given in millimeters relative to the zero pressure state for each image. A Matlab code which is given in Appendix 15 used these text files from the pressure and the geometry to determine a set of parameters and length scales and finally the compression and shear modulus as already discussed in subsection 3.2.2. This Matlab code is based on an existing code of H.M. Wyss in which a number of adjustments have been made. After selecting the text files a commant window will appear where the desired image numbers can be entered, which made it possible to skip

unclear/hazy images or to select only the images at lower or higher pressure states with the use of the complete text files. Some volume and area equations from the original code were replaced with equations which are given in section 3.2.2. Next to the strain definition in the longitudinal (z) direction described with equation 3.10 in section 3.2.2, which is based on the middle part of the cell, other strain definitions in this direction were added in the code to investigate the strain definition behavior. These two other strain definitions are based on the total cell length from the most left to the most right point of the cell (which uses the total cell length) and on the average value between the middle section of the cell and the total cell length. More information about the strain definition is given in appendix 12, just like a performed image quality improvement.

The point selection for each image contained errors because of the manual point selection procedure. To minimize these errors, a few corrections were performed within the Matlab code. At first from all images of one measurement, point numbers two and three were selected and saved and point numbers four and five were selected and saved (numbers are defined in figure 3.7). The set of numbers based on points two and three were used to fit a linear line through all points with an as small as possible value for the sum of squares to define the top wall of the capillary. In the next step all the top points were projected on top of this fitted line to minimize the variation in the vertical image direction as a result of the manual point selection. The same principle was used for points four and five for the bottom wall of the capillary. For the calculation of the angle between the top or bottom wall and the longitudinal direction of the capillary, the average was calculated of the angle at the top and the bottom to take all available points into account. The back and front contact radii were calculated in two ways, (1) with the use of the top points in combination with the middle line and (2) with the bottom points in combination with the middle line and finally the average value of the two was calculated. All steps within the code where average values were calculated have the goal to minimize point variations due to manual selection and to get more reliable parameter values for the modulus determinations.

To get an impression of the difference between the points selected by hand and those which are projected on the fitted lines, a few intermediate steps are plotted within the Matlab code and shown in appendix 9 figure 9.1.

3.8 Error analysis

During the experiment and the image analysis, errors were made which have to be taken into account when representing the final modulus values. First, an error was present because of the pressure set with the fine z-stage. One rotation of this stage was divided into 50 smaller sections and was equal to 0,5 mm (0,01 mm between two smaller sections). Based on this an error was assumed of one fourth of a smaller section, so $\pm 2{,}5e^{-3}$ mm which was equal to $\pm 2{,}5e^{-2}$ Pa for each pressure state. Second, an error was made with the selection of the seven points on each image, where an error was assumed of ± 1 pixel, which is equal to $\pm 0{,}4357$ μm for each point in each direction. The volumetric error percentage can be determined with $\frac{\Delta V}{V} = 2\frac{\Delta x}{R} + \frac{\Delta x}{L}$[9], with Δx the 1 pixel error, L the band length in pixels and R the average band radius in pixels. With the use of $L_{min} = 15{,}9$ pixels, $L_{max} = 105{,}0$ pixels, $R_{min} = 14{,}6$ pixels and $R_{max} = 46{,}8$ pixels (based on the values in appendix 14 table 14.1) the minimal and maximal volumetric error percentages can be calculated, which resulted in percentages of 5,23% and 19,99% respectively.

4 Results

In this chapter, first the cell behavior of both cell lines under normal circumstances are described. Results related to the cell viability and morphology are given. The time dependency and elasticity test are presented for the MDA-MB-231 cell line. Finally the capillary micromechanics results are given for a single measurement and for a set of measurements.

4.1 Cell behavior normal circumstances

Before any conclusions can be made about the two cell lines under experimental conditions, the growth rate and morphology have been viewed under normal cicumstances as given in subsection 3.1.2. The growth rate of both the MDA-MB-231 and the MCF-7 cell lines can be seen in figures 4.1 and 4.2 respectively. A picture of the amount of cells in culture was made after 24, 48, 72 and 96 hours for the MDA-MB-231 cell line and after 12, 72, 96 and 120 hours for the MCF-7 cell line with the use of the Cytomate imaging system. The reason for different time frames was because of issues with the Cytomate imaging system.

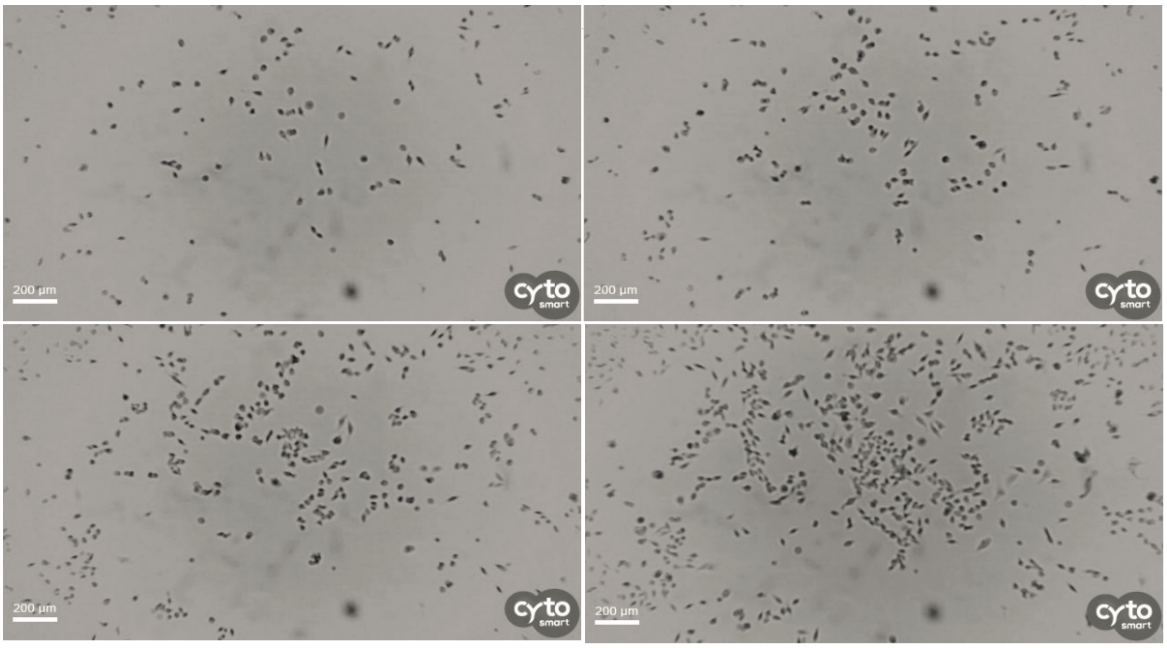

Figure 4.1: *Growth rate of MBA-MB-231 cells within medium. Left top: 24 hours, right top: 48 hours, left bottom: 72 hours and right bottom: 96 hours.*

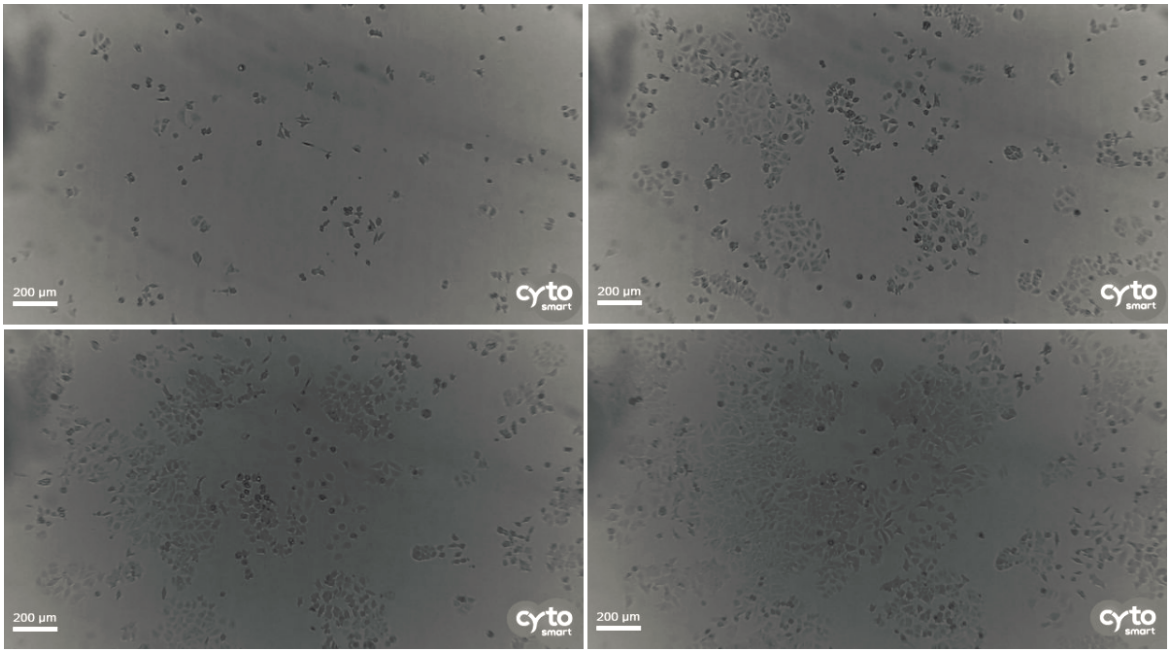

Figure 4.2: *Growth rate of MCF-7 cells within medium. Left top: 12 hours, right top: 72 hours, left bottom: 96 hours and right bottom: 120 hours.*

The morphology of the cells when adhered to the growth surface can be seen in figure 4.3, with left the MDA-MB-231 cell line and right the MCF-7 cell line where both lines show a stretched morphology. After trypsinization the morphology of cells from both cell lines changed to a spherical shape with average cell diameter ranges of 15,81 ± 1,30 μm[34] for the MDA-MB-231 cells and 12,25 ± 1,16 μm[34] for the MCF-7 cells based on literature.

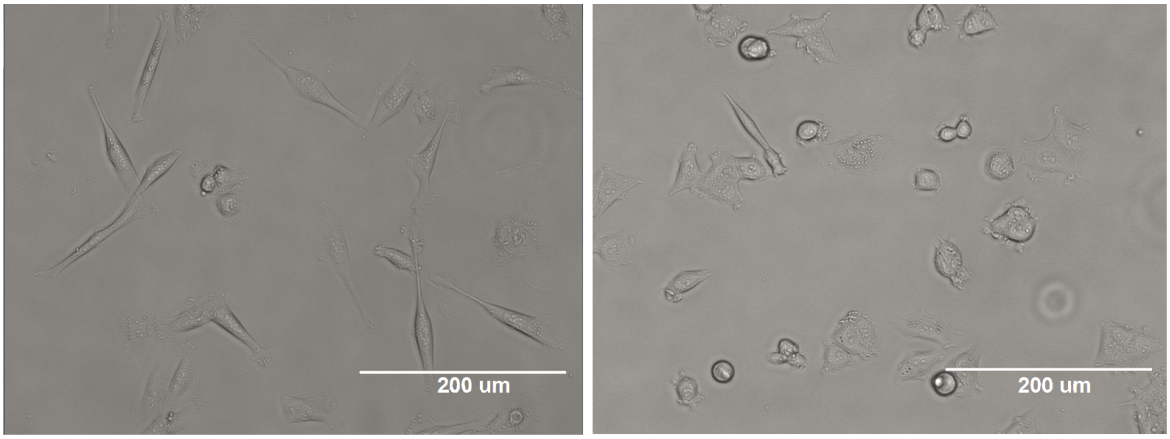

Figure 4.3: *Cell appearance when bound to the growth surface. Left: MDA-MB-231. Right: MCF-7.*

During cell culture each cell goes through a specific cell cycle to duplicate and split and each cycle step may result in a corresponding different mechanical behavior. This cell cycle consists of a G1-phase (cell growth and organel copy), S-phase (DNA copy in nucleus and centrosome duplication), G2-phase (further cell growth, oranel and protein production and reorganization) and the M-phase (chromosome developement and separation and splitting of the cytoplasma)[35]. A unique cytoskeleton for each cell results in small expected mechanical cell variations between cell lines and within a cell line. The passage number is another factor which plays a role in the mechanical behavior, where for example the Young's modulus for

the MCF-7 cells has previously found to decrease, and to be distributed over a smaller value range, when the passage number is increasing from one to ten[36]. These types of mechanical changes may also happen for the MDA-MB-231 cell type and for higher passage numbers.

4.2 Experimental conditions

In this section the results are given of the morphology and viability experiments where information is obtained with the use of nucleocounter measurements and image analysis.

4.2.1 Cell viability

With the use of all the nucleocounter measurements which were done at the start and after a specific time for the different wells, an analysis can be done of the cell viability related to the four conditions described in subsection 3.4. The obtained values can be found in appendix 10, table 10.1. Because of an air bubble within the VIA1 cassette at the start of the uncoated medium situation, the concentration and the theoretical amount of cells per well were unreliable for this measurement. The nucleocounter was unable to count the cells at this air bubble location which resulted in a lower concentration of cells per milliliter compared to the actual case. During the measurement of the PBS uncoated situation of well number one a "too low concentration" error was the result at the nucleocounter. The cell pellet was more difficult to see for the transparent PBS solution, probably because most of the cell pellet was flushed away while removing the liquid above the pellet manually which resulted in a too low concentration for the nucleocounter to measure within the cassette.

The average values for each condition from table 10.1 were placed within two sets of bar graphs, one for the coated and one for the uncoated situation, as given in figure 4.4. In these figures the amount of measurements used to calculate the average is given with the number N and the standard deviations are given with the red line at the top of each bar.

The average values in combination with the standard deviations can be compared by eye, but another way to check if the average values of all groups are significantly different or the same is to perform the one-way analysis of variance test (ANOVA) in combination with a pairwise comparison of the means. This test is done on all data obtained with the VIA1 measurements with the use of the R-commander statistical program and the results can be seen in appendix 11.1, table 11.1. Based on the determined F value of 6,291 which is bigger compared to the F value from the F statistics table with a confidence of 95% and a value of 3,48, the conclusion is that there was a strong evidence of a difference in the mean. Also the calculated p value of 0,00885 which was smaller compared to α=0,05 resulted in a significant difference within the six mean values. Small significant differences were found where all significant differences were coupled to the coated PBS situation which had the biggest standard deviation as given in figure 4.4 and which had one remarkably lower VIA1 measurement value as can be seen in table 10.1. The conditions which were significant different were coupled to each other in figure 4.4 and more details can be found in appendix 11.

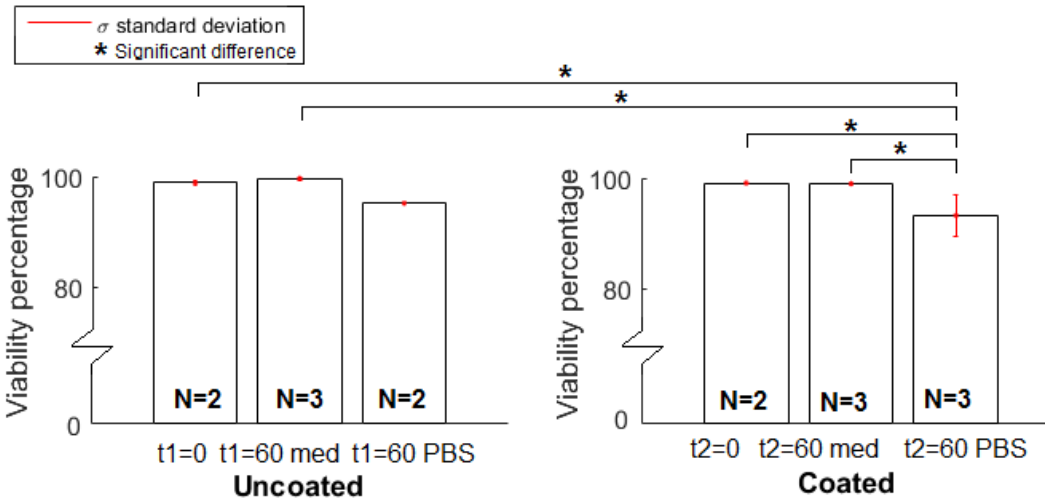

Figure 4.4: *Average viability percentages MDA-MB-231 cells. Left the uncoated wells and right the coated wells. For each situation: left the average viability percentage at the start, middle the average viability percentage for cells in culture medium after one hour and right the average viability percentage in PBS after one hour. All measurements were performed at room temperature at a non-pressurized state. * means a significant difference.*

4.2.2 Cell morphology based on images

The goal of the cell morphology experiment was to investigate the effect on the shape and size of the cells of the presence of BSA, PBS and medium within a period of one hour at room temperature within a non-pressurized environment. At first the length of the 200 μm distance bar was measured in pixels as illustrated in figure 3.5. This length was measured five times which resulted in an amount of (459,03+459,07+459,03+459,01+458,99)/5 = 459,03 pixels and which is related to 200 μm length.

In appendix 10 table 10.2, the cell diameters for the uncoated situation are given and in table 10.3 the cell diameters are given for the coated situation. All diameters were calculated based on the measured pixel distances. As can be seen, measurements at t=0 were done twice each experimental day (one time for the coated and one time for the uncoated situation) for certainty which resulted in 96 single measurement for the starting situation. For t=60 min only 48 single measurements were used for each condition. In figure 4.4 bar graphs are given for the average cell diameters determined based on the image analysis for the different conditions, with in red the standard deviation ranges. Because of the manual selection and size determination of cells in the images, the standard deviation is relatively big. The variation of manual boundary selection and the outliers from each measurement can be seen in figure 4.6 where the diameter values for each condition are represented within a boxplot.

Also for the diameters obtained with the Matlab imdistline function an ANOVA test is done with the R-commander statistical program. With a determined F value of 3,384 which is bigger compared to the F value from the F statistics table with a confidence of 95% and a value of 2,26, the conclusion is that there is a strong evidence of a difference in the mean. Also the calculated p value of 0,00528 which was smaller compared to α=0,05 resulted in a significant difference within the six mean values. The with the Tukey contrast test obtained significant differences are shown in figure 4.5 and can be seen more detailed in appendix 11.2.

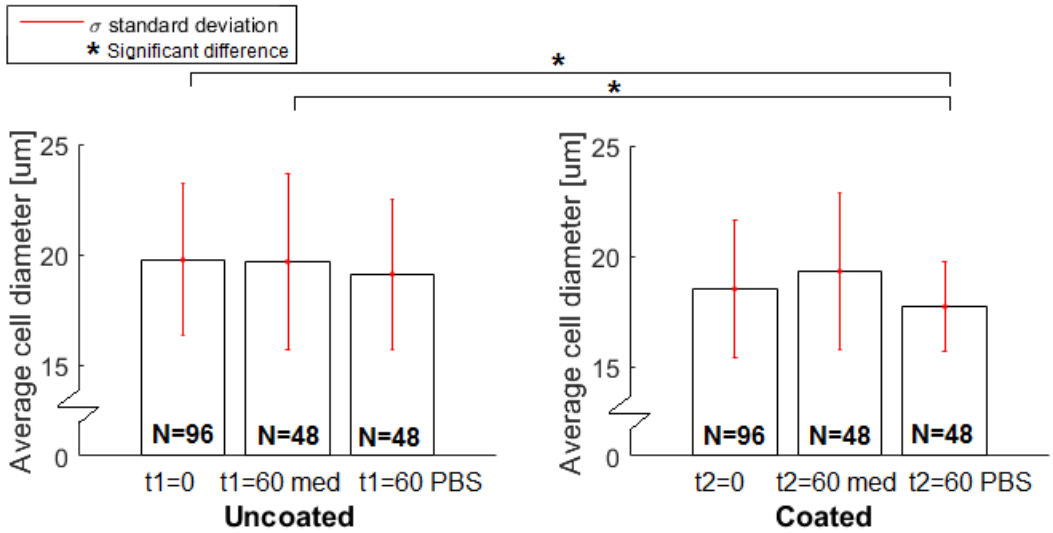

Figure 4.5: *Bar graph with average cell diameters [µm] of MDA-MB-231 cells in standard wells based on image analysis. Left the uncoated wells and right the coated wells. For each situation: left the average cell diameter at the start, middle the average cell diameter for cells in culture medium after one hour and right the average cell diameter in PBS after one hour. * means a significant difference.*

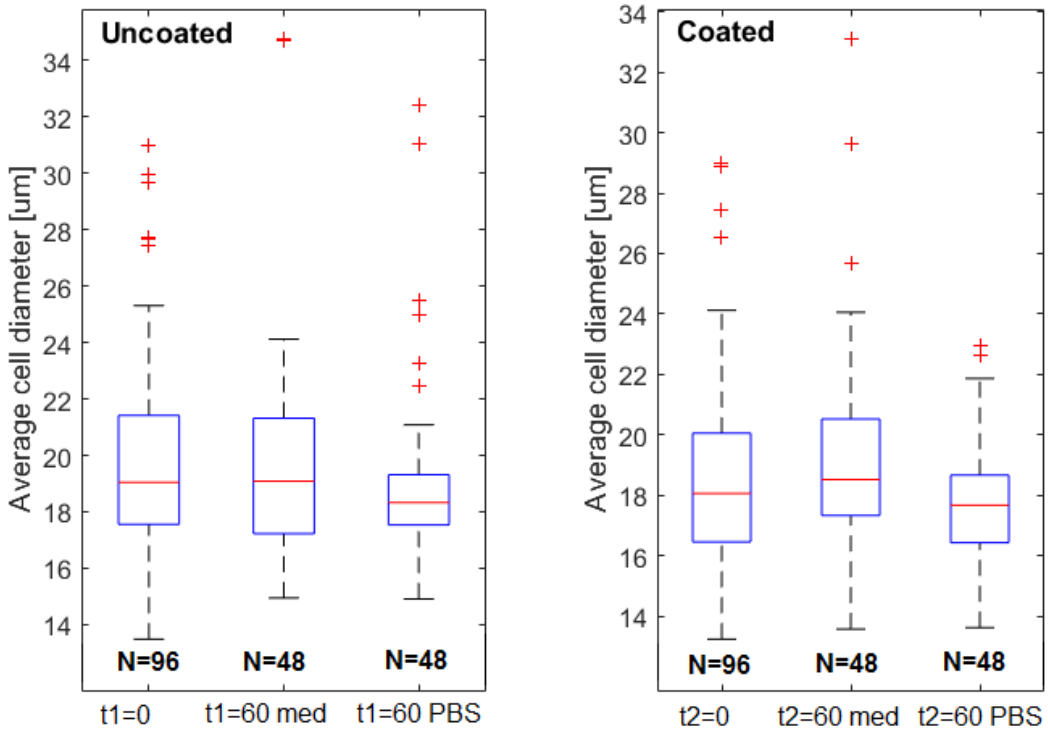

Figure 4.6: *Boxplot with average MDA-MB-231 cell diameters [µm] based on image analysis. Left the uncoated wells and right the coated wells. For each situation: left the average cell diameter at the start, middle the average cell diameter for cells in culture medium after one hour and right the average cell diameter in PBS after one hour.*

4.2.3 Cell diameters based on VIA1 cassettes

During the viability measurement also values for the diameters were obtained which are given in appendix 10 table 10.1 and which were represented within a bar graph in figure 4.7.

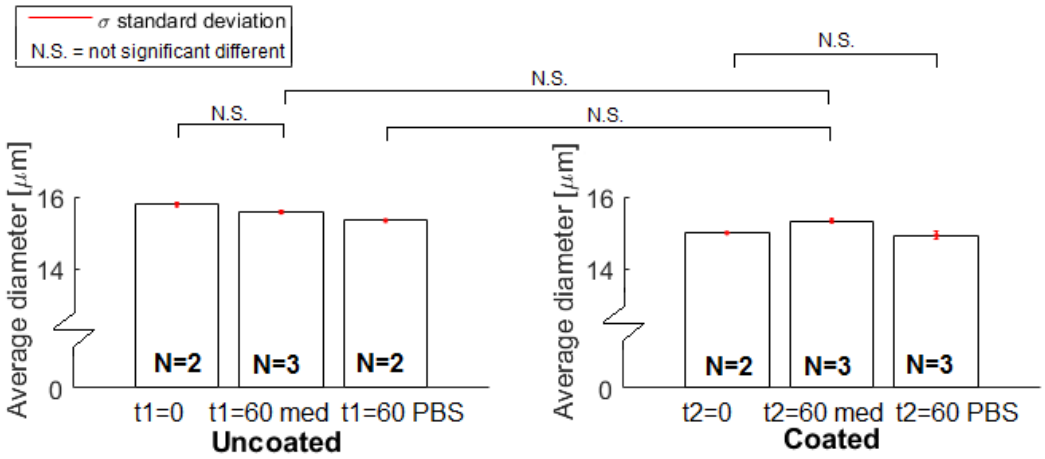

Figure 4.7: *Bar graph with average cell diameters [μm] of MDA-MB-231 cells based on VIA1-cassettes. Left: uncoated situation with left the start values, middle the medium values after one hour and right the PBS values after one hour. Right: coated situation with left the start values, middle the medium values after one hour and right the PBS values after one hour. N.S. means not statistical different.*

The ANOVA and Tukey test on the VIA1 cassette diameters are given in appendix 11.3 table 11.3. An F value was determined of 46,2 which was higher compared to the F value from the F statistics table with a confidence of 95% and a value of 3,48. The calculated p value of 3,78e^{-6} was smaller compared to α=0,05 which resulted in a significant difference within the six mean values. With the use of the p-values of the Tukey test it could be seen that there were significant differences between the most conditions and because of this only the non-significant differences are represented in figure 4.7.

4.2.4 Average diameter differences

Based on figures 4.5 and 4.7 it is apparent that there is a difference between the diameters determined with the imdistline function of Matlab and the values obtained with the nucleo-counter measurement. To find out where these diameter differences came from, a used VIA1 cassette was opened and images were made wiuth the EVOS microscope with transmitted light, with an GFP light cube and with a DAPI light cube which made it possible to visualize the cell stainings which were used within the VIA1 cassette. The visibilty of the cells with the different light cubes can be seen in appendix 10 figure 10.1. For each light cube ten cell diameters were measured in both horizontal and vertical direction distributed over three images for each used light cube. The average diameters and the standard deviations can be seen in figure 4.8 which are based on the measured imdistline values of Matlab as given in appendix 10 table 10.4. Only the DAPI measurements are not represented because a large amount of cells turned out to be not colored in the DAPI stained cell images, which made a good measurement not possible.

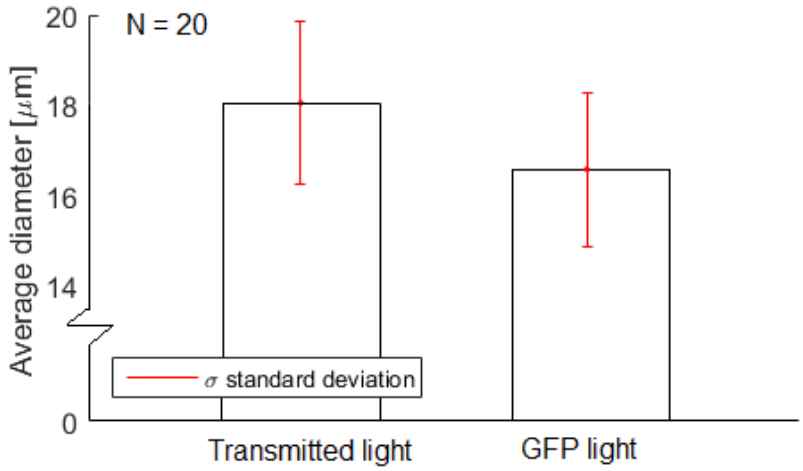

Figure 4.8: *Average diameter values of MDA-MB-231 cells which were stained within a VIA1 cassette and determined based on imdistline measurements of Matlab on images produced with the EVOS microscope for both the transmitted and the GFP light source.*

4.3 Control experiments

In this subsection the results are presented for both the time dependency and elasticity tests for the MDA-MB-231 cell line. The goal of these experiments was to obtain information about the cell behavior without changing the pressure in the tip (time-dependency), to get information about the extent to which the cells behave elastically and to observe effects of friction presence within the experimental setup.

4.3.1 Time dependency

For two MDA-MB-231 cells the pressure was increased until a specific fixed value and from that moment every five minutes an image was made of the cell state until a final time of 45 minutes was reached. This experiment was done twice and the results can be seen in figures 4.9 and 4.10. Within these figures the red lines represent a cell in a 6,22 μm tip at 25 Pa and the blue lines a cell in a 8,40 μm tip at 12,5 Pa. In figure 4.9 the top image represents the strain difference $e_r - e_z$ over the total cell length and in the bottom image the strain difference is defined over the middle part of the cell. In this figure the strain differences are plotted as a function of time and in figure 4.10 the volume and pressure difference are plotted as a function of time. In figure 4.9 the strain is set to zero for both subfigures at the zero-time state and the strain of the other time steps were determined based on this zero-time state.

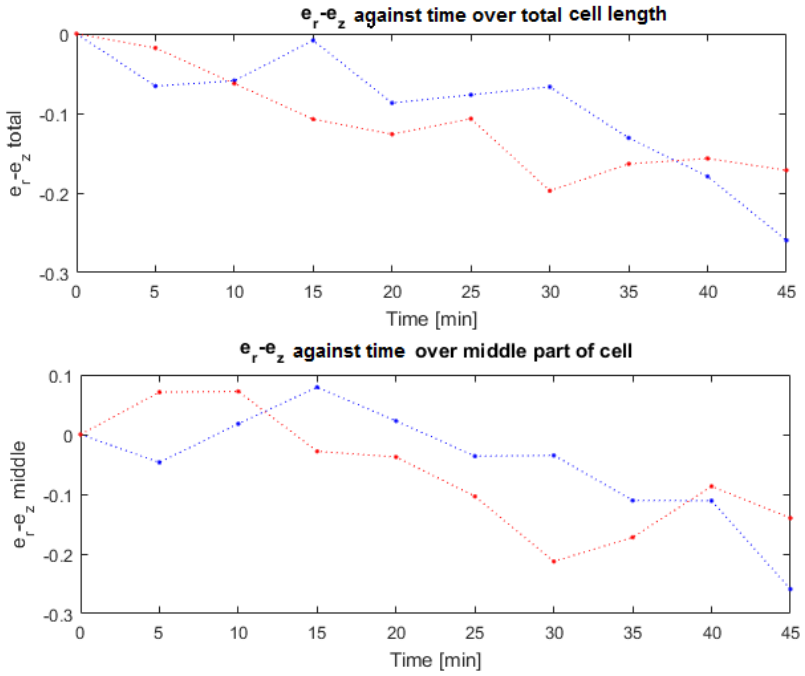

Figure 4.9: *Time effect of MDA-MB-231 cells. The red lines represent a cell in a 6,22 µm tip at 25 Pa and the blue lines a cell in a 8,40 µm tip at 12,5 Pa. Top: $e_r - e_z$ for total cell length and bottom: $e_r - e_z$ for middle part of the cell against the time.*

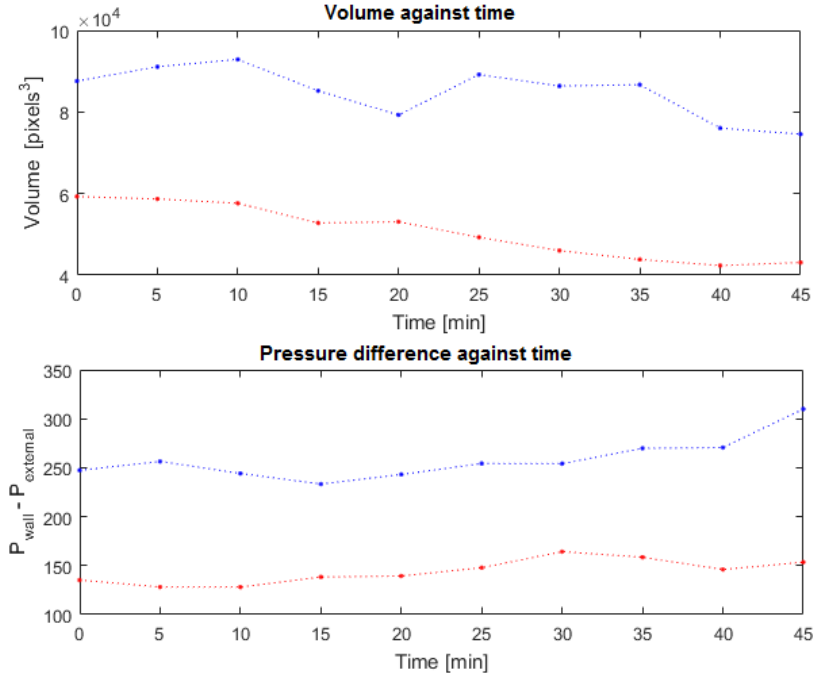

Figure 4.10: *Time effect of MDA-MB-231 cells. The red lines are representing a cell in a 6,22 µm tip at 25 Pa and the blue lines a cell in a 8,40 µm tip at 12,5 Pa. Top: volume and bottom: pressure difference as a function of time.*

4.3.2 Elasticity test

For the MDA-MB-231 cell type a cell was deformed into a capillary tip with a diameter of 5,04 μm with pressure steps of 2,5 Pa until a maximum pressure of 95 Pa was reached. From that moment the same pressure steps were used to decrease the pressure difference. The results of this experiment can be seen in figure 4.11 with left the figure showing the shear modulus with the use of the longitudinal strain over the total cell length, and right the figure related to the compression modulus. The shear and compression moduli are equal to the slope of the measured trends in these figures. The strain over the middle part is not given because it shows the same trend compared to the strain based on the total cell length. The cell shape for a number of pressure differences below zero after the experiment, is given in figure 4.12 where also the deformed shape of the cell is visible when it was disconnected from the capillary walls. It can be seen that the cell was disconnecting the capillary walls between a pressure difference of -20 and -30 Pa. This experiment was also done with a 8,74 μm capillary tip, with a pressure increase till 8,75 Pa with steps of 1,25 Pa. The same behavior was visible and the cell was back at its start location at a pressure difference of -6,25 Pa where the cell was almost round shaped when not touching the walls anymore.

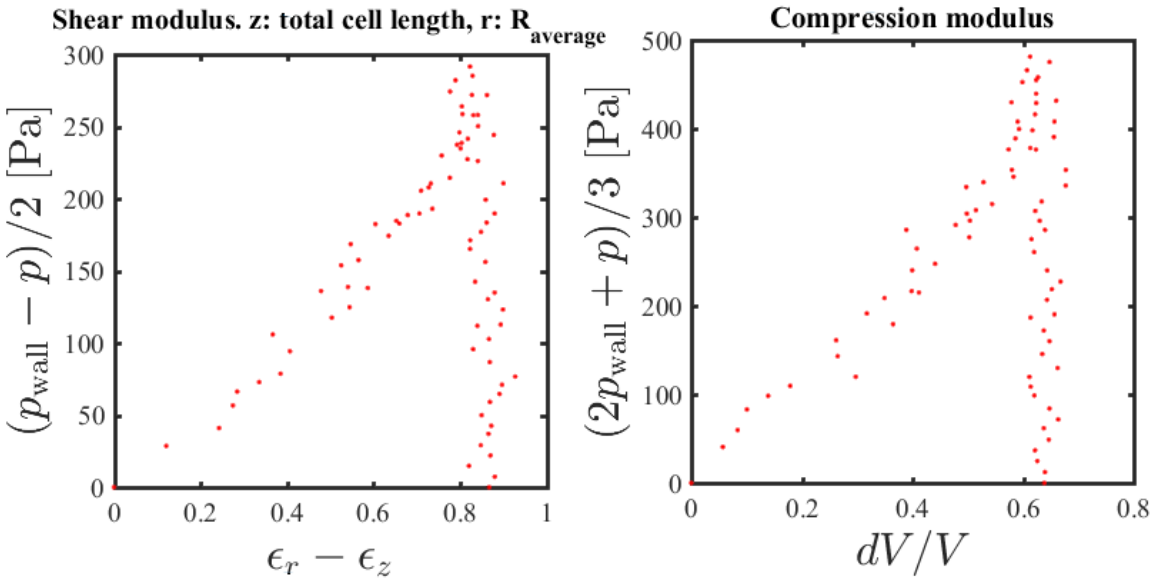

Figure 4.11: *Elasticity test MDA-MB-231 cells. Left the figure related to the shear modulus with the longitudinal strain related to the total cell length. Right the figure related ot the compression modulus.*

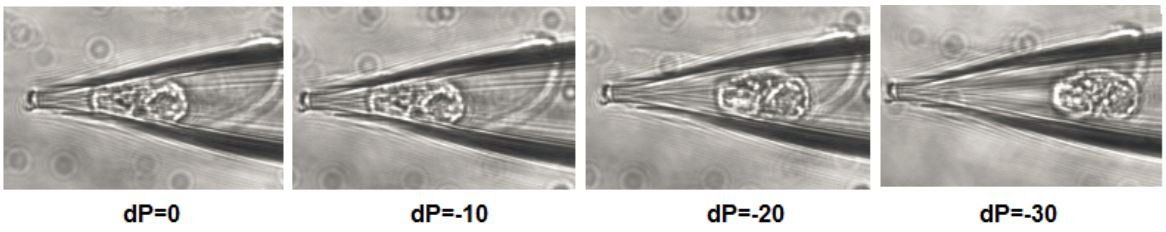

Figure 4.12: *Elasticity test negative pressure difference. MDA-MB-231 cell at a pressure difference from left to right of 0, -10, -20 and -30 Pa.*

4.4 Shear and compression modulus determination

This subsection presents a measurement example for both cell lines where the shear and compression modulus are determined. The shear and compression modulus values are analyzed and compared, and finally the elastic modulus and Poisson ratio are calculated.

With the use of the Matlab code values for the shear and the compression modulus were generated for each cell measurement. An example of the MDA-MB-231 cell line results is given in figure 4.13, where a 5,04 μm tip diameter was used. An example of the MCF-7 cell line results is given in figure 4.14, where a 7,33 μm tip diameter was used.

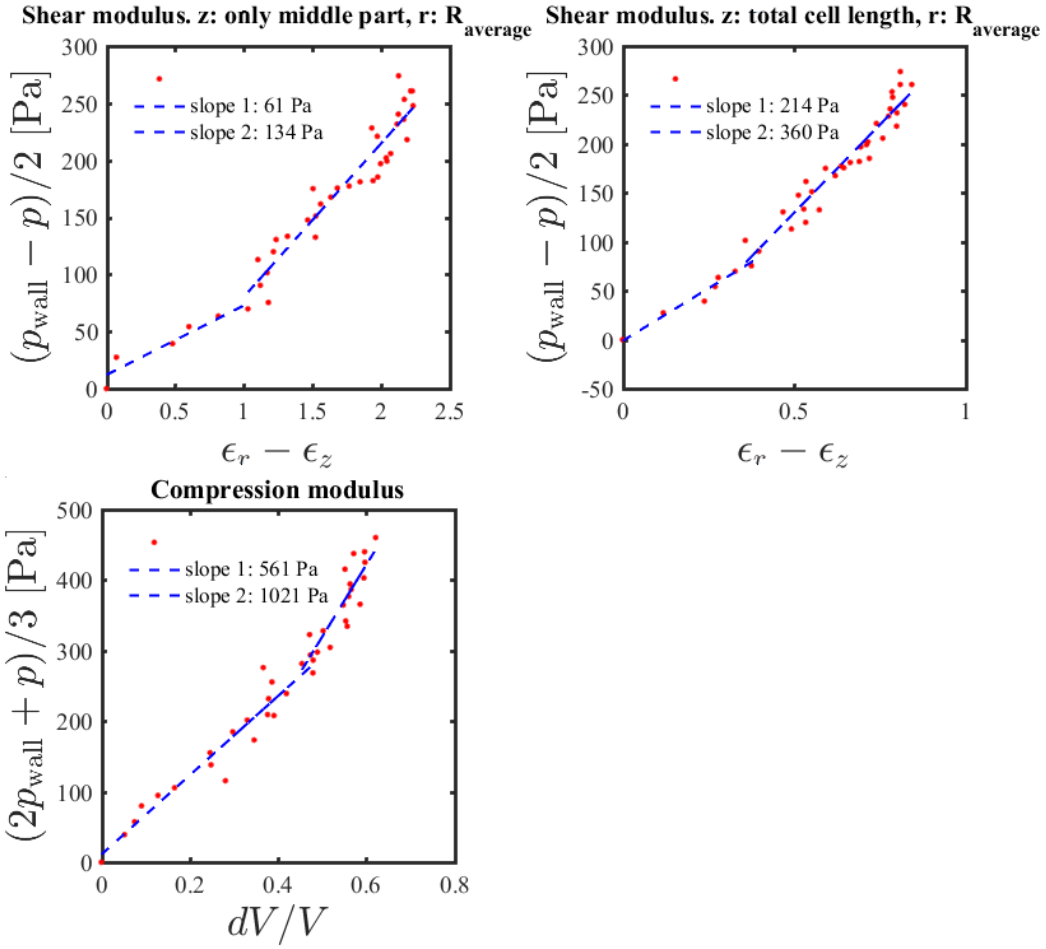

Figure 4.13: *Shear and compression modulus of MDA-MB-231 cell with a 5,04 μm tip diameter and a maximum applied pressure of 95 Pa. Left top: shear modulus with strain in longitudinal direction based on middle part. Right top: shear modulus with strain in longitudinal direction based on total cell length. Left bottom: compression modulus.*

Each fit for the MDA-MB-231 cell line is separated into two parts, one for the small deformations at lower pressure differences and one for the bigger deformations at higher pressure differences, which resulted in two values for each modulus. The reason for two linear fits instead of one linear fit is because of the points which showed a non-linear trend and where this non-linear trend can be separated in roughly two linear parts. When all points were almost on the same line within an analysis, the same value was used for the modulus value for both the small and the bigger deformations to make it possible to compare all measurements later

on. The transition from the first to the second fit part was determined by trial and error until the fits visually matched the points in an by eye good way for both the shear modulus and the compression modulus. For the MCF-7 measurements, only a single fit line was used because of the small applied pressures and the corresponding linear elastic behavior. When a point was extremely different from all the other points then it was not used for fitting due to a probably inaccurate point selection during the creation of the geometry file. In appendix 13 all measured data graphs are given for both cell lines. For a better overview, the tip diameter, maximal pressure and the modulus values are summarized in tables 4.1 and 4.2 for all finally used cell measurements.

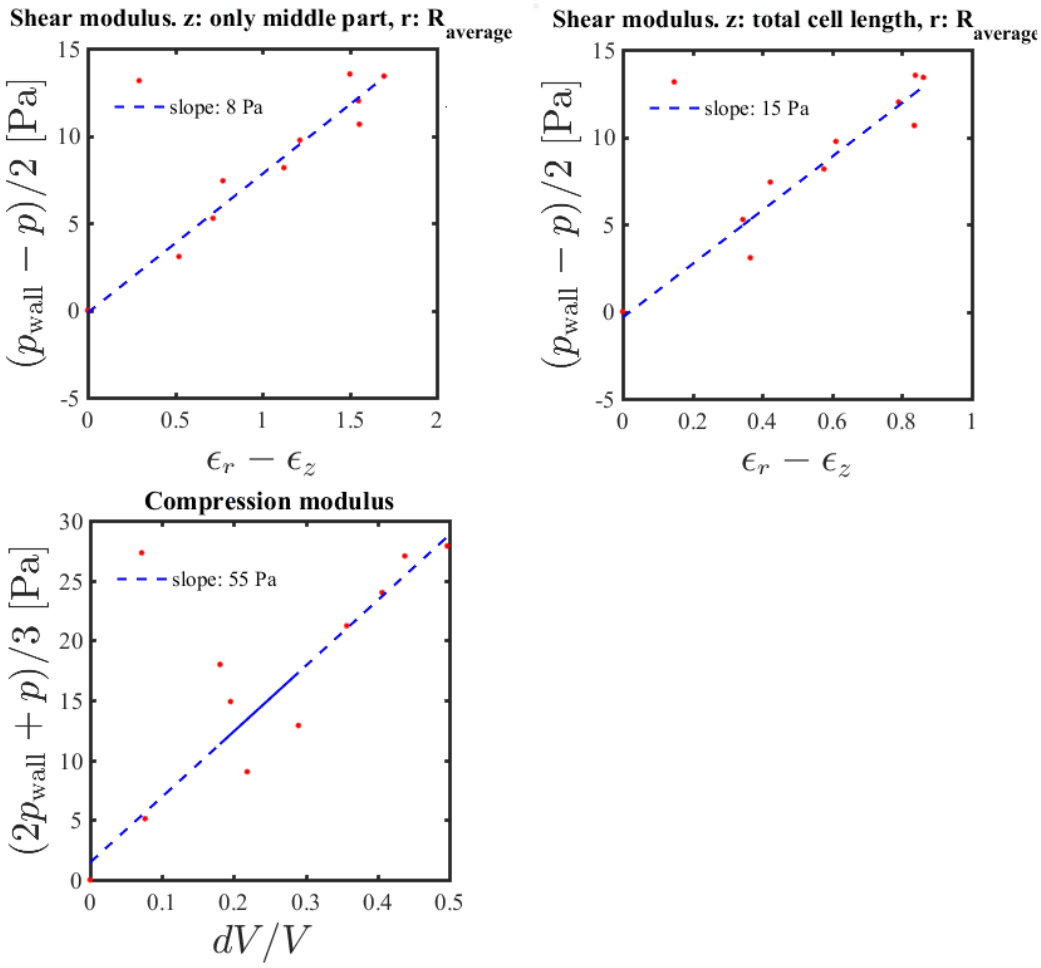

Figure 4.14: *Shear and compression modulus of MCF-7 cell with a 7,22 µm tip diameter and a maximum applied pressure of 10 Pa. Left top: shear modulus with strain in longitudinal direction based on middle part. Right top: shear modulus with strain in longitudinal direction based on total cell length. Left bottom: compression modulus.*

Table 4.1: *Shear and compression modulus values for the MDA-MB-231 cell line. d_{tip} is the tip diameter, p_{max} the maximal applied pressure, K_1 and K_2 represent the compression modulus, G_{1m} and G_{2m} the shear modulus with the strain in longitudinal direction of the middle part and G_{1t} and G_{2t} the shear modulus in the longitudinal direction of the total cell length. For all values, number 1 is related to the low strain situations and number 2 to the high strain situations.*

#	d_{tip} [μ**m**]	p_{max} [**Pa**]	K_1 [**Pa**]	K_2 [**Pa**]	G_{1m} [**Pa**]	G_{2m} [**Pa**]	G_{1t} [**Pa**]	G_{2t} [**Pa**]
1	5,04	95	561	1021	61	134	214	360
2	6,97	70	305	1685	214	214	124	124
3	5,88	100	790	1330	100	194	301	577
4	5,88	100	1279	6172	250	250	999	999
5	9,07	26	124	376	43	79	143	337

Table 4.2: *Shear and compression modulus values for the MCF-7 cell line. d_{tip} is the tip diameter, p_{max} the maximal applied pressure, K represents the compression modulus, G_m the shear modulus with the strain in the longitudinal direction of the middle part and G_t the strain in the longitudinal direction of the total cell length.*

#	d_{tip} [μ**m**]	p_{max} [**Pa**]	K [**Pa**]	G_m [**Pa**]	G_t [**Pa**]
1	7,22	10	55	8	15
2	7,22	9,5	22	2	6
3	7,22	4	59	5	7

The averages and standard deviations of the moduli for the MDA-MB-231 cell line are given in figure 4.15 and for the MCF-7 cell line in figure 4.16 and the corresponding values can be seen in table 4.3. For the MDA-MB-231 measurements in table 4.1 it is clear that the fourth measurement has much higher values compared to the other measurements. Because it is unknown if these higher values are the result of intrinsic cell behavior or as a result of an experimental error, the average values and standard deviations are given with and without this measurement to see the differences.

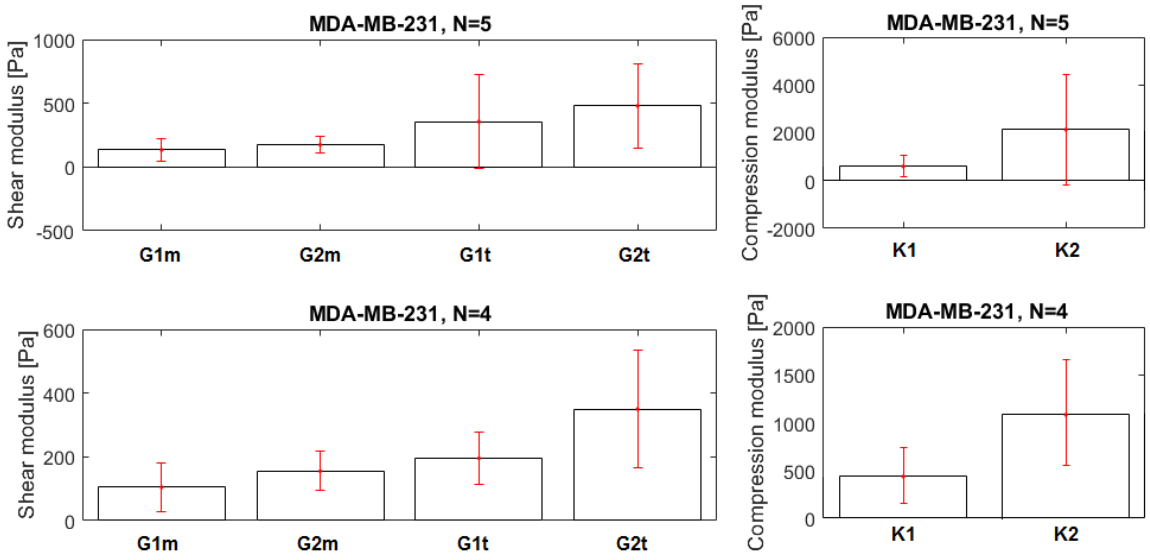

Figure 4.15: *MDA-MB-231 shear and compression modulus including the standard deviations. The top graphs show results taking into account all five measurements, in the bottom graph, measurement number four is excluded from the analysis. G1m and G2m are the shear modulus for the strains over the middle part, G1t and G2t the shear modulus for the strains over the total cell length and K1 and K2 the compression modulus. For all values, number 1 is related to the low strain situations and number 2 to the high strain situations.*

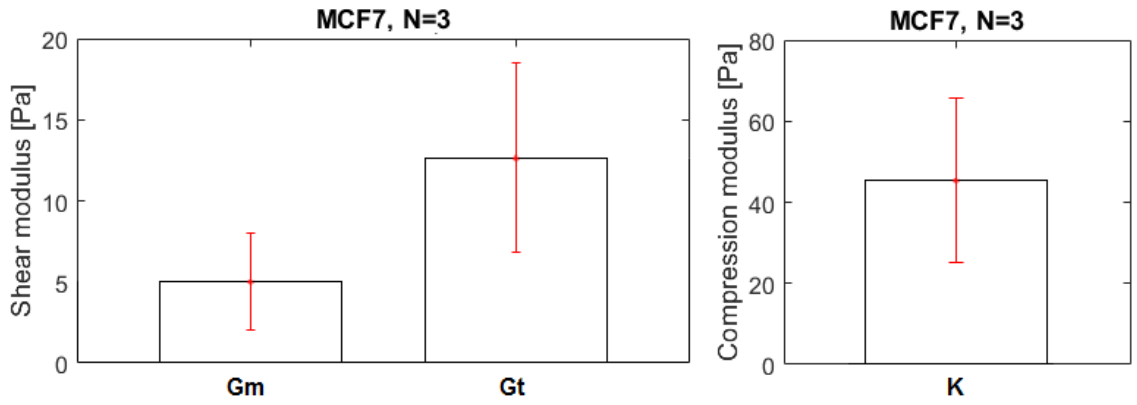

Figure 4.16: *MCF-7 shear and compression modulus including the standard deviation. Three measurements with Gm the shear modulus for the strain over the middle part, Gt the shear modulus for the strain over the total cell length and K the compression modulus.*

Table 4.3: *Average and standard deviation values of the moduli for the MDA-MB-231 cell line with N=5 (including all measurements) and N=4 (excluding measurement four) and for the MCF-7 cell line with N=3.*

Modulus information	**N**	**Cell type**	**Average modulus [Pa]**	**Standard deviation [Pa]**
G1m	5	MDA-MB-231	133,6	93,0
G2m	5	MDA-MB-231	174,2	67,8
G1t	5	MDA-MB-231	356,2	366,0
G2t	5	MDA-MB-231	479,4	331,8
K1	5	MDA-MB-231	611,8	450,4
K2	5	MDA-MB-231	2116,8	2317,4
G1m	4	MDA-MB-231	104,5	76,8
G2m	4	MDA-MB-231	155,3	61,2
G1t	4	MDA-MB-231	195,5	80,3
G2t	4	MDA-MB-231	349,5	185,2
K1	4	MDA-MB-231	445,0	291,6
K2	4	MDA-MB-231	1103,0	555,4
Gm	3	MCF-7	5	3
Gt	3	MCF-7	12,7	5,9
K	3	MCF-7	45,3	20,3

With the use of the average values for each situation the elastic modulus and the Poisson ratio can be calculated using equations 3.13 and 3.14. The results of these values can be seen in table 4.4, where for the shear and compression modulus the average values are used which are given in table 4.3.

Table 4.4: *Elastic modulus and Poisson ratio based on average shear and compression modulus values for the different situations.*

Cell type	**N**	**Slope specification, 1th or 2nd**	**Strain definition**	**Elastic modulus E [Pa]**	**Poisson ratio ν [-]**
MDA-MB-231	5	1th	Total	894,9	0,256
MDA-MB-231	5	2nd	Total	1137,2	0,395
MDA-MB-231	5	1th	Middle	373,7	0,398
MDA-MB-231	5	2nd	Middle	508,6	0,460
MDA-MB-231	4	1th	Total	511,6	0,308
MDA-MB-231	4	2nd	Total	948,3	0,357
MDA-MB-231	4	1th	Middle	290,7	0,391
MDA-MB-231	4	2nd	Middle	445,0	0,433
MCF-7	3	-	Total	34,8	0,372
MCF-7	3	-	Middle	14,5	0,447

5 Discussion

Within this section the measurement results will be discussed and compared to the literature. First, the cell behavior under normal circumstances is discussed, followed by the observations related to the experimental conditions, the measurement protocol, the strain definitions, image quality improvement and the error analysis. The results of the time dependency and the elasticity experiment are discussed next. Finally, the shear and compression modulus results are viewed more critically.

5.1 Cell behavior normal circumstances

As can be seen in figures 4.1 and 4.2 the cells can be cultured for at least four days with a start ratio of 1:10 before a new passage was needed. It must be taken into account that a higher start ratio (or a 1:10 ratio from a flask which had a higher confluence value) will reach a high confluence percentage sooner. While culturing, the cells can obtain multiple growth situations dependent on the start ratio within the flask. When too few cells are placed within a flask, cells stretch more than normal to find other cells to communicate with which results in a less optimal culture environment. When too many cells are placed in the flask at the start, cell accumulations result in a shorter time. Cells in the middle were not able to grow in an unstressed environment because of very close surrounding neighbour cells and results possibly in cell dead[37]. The growth speed is also dependent on the quality of the medium which was present in the flask, when the medium was added during the cell passaging it had a red color which meant that the medium was new. The change in color is the result of a pH indicator insde the culture medium where the pH value is coupled to the color and in this way the state of the culture medium. During the cell growth, cells use the nutrition components in the medium and cells give off waste components which resulted in an orange and in the worst case a yellow medium color. When there were too many waste components and too few nutrients within the medium, the cells grew slower compared to the fresh medium situation because of a change of a metabolic process change.

When looking to figure 4.3 it can be seen that the MDA-MB-231 cell line has a more stretched morphology when attached to the growth surface compared to the MCF-7 cell line. Based on the outer diameter ranges, variations in the nucleus diameter, differences in each cell cytoskeleton structure, the passage number and the cell cycle state, the expectation was that the mechanical properties were different between both cell lines, but also within a single cell line for the measured cells. Looking more critically at the cell cycle steps explained in section 4.1, a further stage of the cell cycle results in a bigger cell size and an expected locally more flexible behavior during the last part of the M-phase where the cytoskeleton is rebuilding and where the cell is splitting.

Based on the growth speed images, a duplication time around 24 hours can be seen. Based on this duplication time only a very small cell change was expected as a result of the cell cycle during an experiment, which lasted between one and two hours dependent on the chosen number of pressure steps. During an experiment it is still unknown in which cell cycle phase the measured cell exactly is.

5.2 Experimental conditions

Based on the theoretical average diameters given in section 4.1 of both cell lines in combination with the invasion investigation of H. Eslami Amirabadi et al.[22] where matrix diameters of 3.6±0,3 μm were used [22], strain values around -0,74 can be expected on average in the radial direction (negative because of radius which must decrease upon entering the matrix). These strain values are only based on the radial direction and are only a rough indication of the strain magnitudes. In practice also factors like volumetric deformations and the strain in the longitudinal direction will play a role. Nevertheless, based on these strains the indication can be made that the smaller cell deformations have the main interest to obtain the mechanical properties and that the chosen 7 μm (± 2 μm) diameter for the tip of the capillaries were small enough to determine the lower deformation range.

When looking at the VIA1 cassette values given in appendix 10 table 10.1, conclusions can be made about the effects on the cells of the different conditions. The amount of cells counted in the wells were in most cases lower compared to the theoretical cell amount because of cells lost between different process steps. When looking at the concentrations within the wells of a single condition, the measured values are relatively close to each other. As first some cells will be left in the pipette which is used to transport the cells from the tube to each well, here also a pipetting error will take place where the amounts are not exactly the same for each well. After one hour the cells were transported from the wells to a tube for each well. Also during this step it was possible that some cells were left at the well or within the pipette tip. The biggest amount of cells could be lost after the centrifuge step where the medium or PBS was manually removed from above the cell pellet. In medium the cell pellet was well visible, but in the PBS case the cell pellet was more difficult to see because of the transparency of the PBS.

Looking at the bar graphs in figure 4.4 showing viability for both the uncoated and coated case the average values for the starting conditions and for the cells in medium were the highest and on average above 98%. The cases with cells in PBS have average values of 95% and 93% for the uncoated and coated conditions, respectively. All viability values have a relatively low error bar. Overall all viability percentages are high, which means that BSA, medium and PBS have no notable effect on the viability of the cells within a one hour period at room temperature in a non pressurized environment. Looking to the ANOVA and Tukey contrast test significant differences were found only in the coated PBS situation, but for both the coated and uncoated situation this solution had still a high viability percentage.

Based on the bar graph and the boxplot representation of the determined cell diameters given in figures 4.5 and 4.6 respectively, the conclusion can be made that also for the cell morphology no noticable effect can be found of the use of PBS, BSA and medium at room temperature in a one hour timeframe at an unpressurized cell state. This conclusion can be made based on all the overlapping standard deviation ranges, the average values of the cell diameters which are close to each other (in both the bar graph and boxplot representation) and the test statistics where only the coated PBS situation had significant differences, but which is still relatively close to the other diameter values from the other situations.

Given the diameter values obtained with the VIA1 cassettes the average values of all conditions are almost on the same line in combination with very small standard deviation bars. Based on the test statistics there are multiple significant differences in the mean values between the groups, but still the differences can be interpreted as small because of average diameters variating from 14,93 μm for the coated PBS situation to 15,75 μm for the uncoated situation at the start. When comparing the cell diameter values based on the image analysis

and based on the nucleocounter results, there is a remarkable difference. The average values of all the measurements together results in a diameter of 19,0 μm and 15,3 μm for the image method and the nucleocounter method, respectively. The difference of the diameters can be explained by the analysis method of the VIA1 cassette which uses "acridine orange" and "DAPI" fluorescent cell stainings [38] which will react mostly with the nucleus of the cells and less with the cell periphery. Acridine orange emits a green fluorescent color when the staining is bound to dsDNA and red when bound to RNA or ssDNA when exposed to the GFP light source[39]. DAPI emits a blue fluorescent color when exposed to the DAPI light source[40]. Both fluorescent stainings react with the nucleus or with nucleic acids, while the image analysis with Matlab uses the cell membrane boundaries of the cells. The difference can be seen in figure 4.8, where the transmitted light situation results in a higher average cell diameter compared to the measurement on the same cells based on the acridine orange staining with the GFP light cube which is used by the nucleocounter.

5.3 Experimental protocol

During the measurements it was difficult to catch a single cell within the capillary tip because of the adherent behavior of the cells, which was observed as a much bigger problem for the MDA-MB-231 cell line compared to the MCF-7 cells. This indicates that the MCF-7 cell line adhere less to the capillary walls and to other cells within the capillary. When the fluid velocity in the capillary was too low cells tried to stick to the walls although the walls were coated with a BSA solution. Most of the time only a height change with the use of the z-stages was not enough to disconnect the cells from the walls, so a pressure by hand was needed. By adding a pressure by hand on the input syringe the cells easily moved too fast with cell clogging and cell damage at the tip as the result. A damaged cell created immediately a sticky behavior inside the capillary tip which made the device useless when this happened during the cell catching phase of the experiment. Another difficulty was the presence of air, despite the check for air bubbles sometimes air was found in the capillary. When air was present within the neelde, tube or connection parts the air bubbles were compressing in an easier way compared to the PBS solution with the cells, which resulted in a final pressure at the tip which was unrealiable.

5.4 Strain definition and image quality improvement

The strain in the middle part of the cells is better defined because of the four selected points between the cell and the capillary wall, although the length in the middle part is very small at the start at which the zero pressure state is defined and when the cell is just touching the walls of the capillary. With the use of this very small start length, a relatively high strain was the result at higher pressure states (till $e_r - e_z$ strain values of five). With the use of the total cell length, the longitudinal length at the start was higher and $e_r - e_z$ values till one were the result at higher pressure states which was more realistic.

Based on the better contrast a final magnification of 32x was used for all experiments. When looking at figure 12.1 A it can be seen that the edges of the capillary and the edges of the cell were not perfectly visible. At both the top and the bottom side of the capillary a more black area is visible in which the real boundary is located and around the cell a vague region can be seen. Still the images were good enough for the analysis, where for each cell measurement and for each image the boundary of the walls of both the capillary and the cell were chosen in the same way to make all measurements comparable with a higher reliability. Creating

images with a better quality was difficult because of 3D shapes, curved structures, materials at different heights with different refraction indexes and a focus point which was different at each location at the tip because of a height difference over the length of the tapered area of the capillary. Nevertheless the microscope focus was targeted on the cell located in the middle of the capillary and a clear image was the case at the start, the focus was changing over the capillary length because of a not perfectly horizontal orientation of the capillary compared to the microscopic objective.

5.5 Error analysis

At first when looking at the estimated error as a result of the pressure set with the small z-stage, it can be concluded that the error is minimal compared to the errors introduced by pressure steps which are used during the measurements. The smallest step which was used within the pressure was 0,1 mm which was equal to 1 Pa, resulting in a pressure set error of only 2,5%.

A minimal volumetric error of 5,23% and a maximum volumetric error of 19,99% was determined based on all used measurements. Because of the presence of this error within each image and within each cell measurement still the compression modulus was determined in a good way and results were well comparable. The maximal volumetric error is based on the most extreme values and is assumed as acceptible.

Within the Matlab code the assumption was made that the capillary consists of straight walls at the tip location. In practice there will be a small curved shape as can be seen in figure 4.12. This more curved shape is mostly visible the closest to the tip location. When looking at figure 9.1 it can be seen that the selected poins are almost on a straight line and that the variation in the radial direction is minimized by projecting all the points on the fitted line. The error because of the needle shape is because of these reasons determined as minimal.

5.6 Time dependency

The strain for both strain definitions used, the volume and the pressure difference behaviors are given for two cells at a constant pressure state over the time in section 4.3.1. As can be seen in figures 4.9 and 4.10, for both cells the same behavior is visible when looking at the total period (when looking at smaller periods, the points are fluctuating more which can be the result of image analysis errors). First, it can be seen that for both strain definitions the strain difference decreases with time, which is the result of an increasing strain in the z-direction. Based on this the conclusion can be made that over the time the cell will elongate in the tip direction. Over time the volume decreases and the pressure difference increases, where the higher pressure deforms the cell somewhat which explains the strain increase and where the cell is compressed which resulted in the decrease in volume. Based on this it is most probable that over time the cell deformation is not only the result of the change of the external applied pressure, but also a result of a time effect. One reason for this can be the evaporation of the PBS in the liquid reservoir of the capillary device as a result of the temperature with a value of 37°C, still this influence is observed as minimal. Another probable reason is a creep behavior of the living cell over time where the cell has an active behavior and moves on its own into the tip or reorganized its own internal cytoskeletal structure. A last probable reason for the decrease of the volume of the cell can be a result

of the continuous pressurization of the cell, where over the time small amounts of water will pass through the membrane of the cell[9].

5.7 Elasticity test

The mechanical response to a pressure increase and subsequent decrease is given in figure 4.11. For a full elastic behavior without cell adhesion or friction the expectation was that the cell moves back to its start location when the pressure difference was moved back to zero and that the cell was again round-shaped right after the experiment. Looking at figure 4.11 it can be seen that at a zero pressure difference the cell was almost not moved back and that the volume and the strain difference were almost the same as the the maximum values of the increasing pressure phase. When decreasing the pressure difference below zero the cell slowly moved back as can be seen in figure 4.11, until the cell was disconnected from the walls where it was visible that the cell was plastically deformed or needed a longer time to recover to its original shape after the experiment as is given in figure 4.12. The second measurement also resulted in a negative pressure difference needed to disconnect the cell from the capillary wall, but this time the cell was round shaped again ater the experiment. Two conclusions can be made from these measurements. First, cell adhesion and friction play a role because of the relatively high negative pressure which was needed to move the cell back to its original position. Second, the cell will deform plastically at least when the pressure difference on the cell becomes too high, and will deform back to its original shape when the pressure difference stays within yet unknown value ranges.

5.8 Shear and compression modulus

When looking at the typical measurement in figure 4.13 and the MDA-MB-231 measurements in appendix 13 it can be seen that in most cases for both the shear and the compression modulus a strain stiffening effect is visible, where the moduli values resulted in a higher value with an increasing strain beyond a certain strain value. A possible reason for this can be the contribution from the nucleus which plays a role when the cell is exposed to higher deformations and where not only the cytoskeletal components around the cell nucleus are deforming. That this strain stiffening effect was sometimes visible and sometimes not can be the result of the cell variations which are described in section 4.1, where each cell may behave in a different way at certain circumstances. Another cell cycle state may be for example a reason for the absence or presence of the strain stiffening effect. When looking at the MCF-7 measurements in figure 4.14 and in appendix 13 this strain stiffening effect was not visible. This does not mean that the strain stiffening effect does not happen at this cell type, but it was not visible with the deformations applied on the cell during the experiments within this investigation. From table 4.2 and the experimental experience it is remarkable that the MCF-7 cells deformed into the capillary tip at much lower pressure values compared to the MDA-MB-231 cells. This behavior of the MCF-7 cell line was not only observed from the obtained modulus values, but this was also clearly visible during the experiment.

Based on figure 4.15 and table 4.3 it can be seen that the average values of the shear modulus for both MDA-MB-231 and MCF-7 are higher for both the small and the big deformation parts, when the strain definition using the total cell length was used. When looking at the two sets of values for the MDA-MB-231 cell type it can be seen that by excluding the one measurement with the more extreme values, a decrease of all average moduli and standard deviation values is the result. This indicates that only a single measurement which is a bit

different compared to the other values has immediately a big influence on the final results.

When comparing both cell lines it can clearly be seen that the MDA-MB-231 has bigger modulus values for both strain definitions when comparing only the values at the smaller deformations. Without a further investigation of the MCF-7 cell line the results cannot be fully trusted. All three MCF-7 measurements were done with the same tip and when there was a measurement error during the experiment or when there was more exceptional cell behavior, it is not possible to recognize this with the data presented in this investigation. When multiple tips and multiple cell passages are used, multiple measurements can be performed to recognize the possible special behavior. When more measurements are performed on the MCF-7 cell line the comparison with the MDA-MB-231 cell line will be more reliable.

Looking at table 4.4 it can be seen that the elastic modulus of the MDA-MB-231 cell line has higher values compared to the MCF-7 cells. When comparing the first with the second slope, the second slope has higher values for all cases. When looking at the Poisson ratio values it can be seen that all results have values above 0,25 and below 0,5, which is in the range of the more deformable materials.

5.9 Comparison with literature

At first when looking back at the investigation to H. Eslami Amirabadi et al. an observation was done where MDA-MB-231 cells migrated further into the fabricated matrix after three days compared to the MCF-7 cells with the use of a stimulating gradient[22]. Based on this, lower modulus values were expected for the MDA-MB-231 cell line to have less resistance to volume or shape changes and to migrate more easily into the matrix compared to MCF-7 cells. The results within this investigation suggest the opposite, where the modulus values for the MDA-MB-231 cell were found to be higher. On the other hand the difference of the amount of migration can also be the result of an active behavior of the different cell lines, where the cell is crawling into the matrix (and within this investigation crawling further into the capillary, towards the tip) on its own without a stimulation or external influence.

In an investigation by L. Graziano et al. an elastic modulus is given for an average breast tumor with a modulus value of 4049±938 Pa[41], which is larger compared to the calculated values in table 4.4. Because of the wide variety of cancer cell types this is more a general indication of the elastic modulus instead of a value which can be compared properly with the determined values within this investigation. Another investigation shows elastic modulus values related to the distribution of cells where the modulus is measured using atomic force microscopy. The results for the MCF-7 and MDA-MB-231 cells can be seen in figure 5.1[42]. Comparing the results of the small deformations from table 4.4 with figure 5.1 the values of both strain definitions are within the range of realistic modulus values. The obtained elastic moduli of the MDA-MB-231 cells represent a lowest value of 290,7 Pa and a highest value of 894,9 Pa for the small deformations and small pressures, where the most elastic moduli values are closer to the minimal value and in this way in accordance with the distrubution in figure 5.1. When comparing the elastic modulus of the MCF-7 cell line of 34,8 Pa and 14,5 Pa with this figure, the measured elastic modulus values are at the minimal boundary.

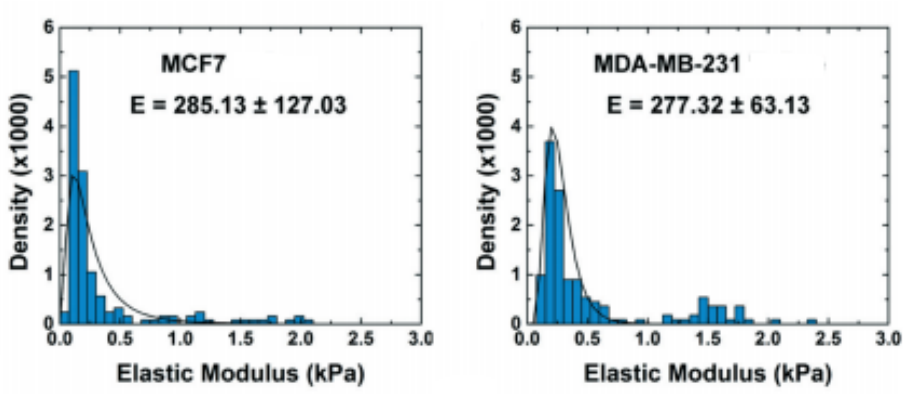

Figure 5.1: *Cell density against elastic modulus. Left: MCF-7 cells. Right: MDA-MB-231 cells* [42].

6 Conclusion

The work described in this thesis illustrates the importance of measurements of mechanical properties of single cells in the context of the diagnosis, treatment and better understanding of diseases and/or disease phases. The cell lines investigated are the adherent MDA-MB-231 and MCF-7 breast cancer cell lines. In an earlier study, these cells were used in an invasion experiment, observing cell migration through a matrix under influence of a chemical stimulus[22]. To better understand the observed behavior in the earlier study, it is interesting to know whether the mechanical properties of the cells play a role.

To measure mechanical cell properties multiple methods can be used. For this investigation the capillary micromechanics method[27] was chosen because of the possibility to do single cell analysis and because it can provide quantitative information on elastic moduli. With this method a cell is trapped in a glass capillary with a short taper and a diameter of 7 μm ($\pm$ 2 μm) at the tip. The capillary is coated with BSA to minimize friction forces. By increasing the height of a fluid reservoir connected to the inlet of the capillary, the pressure was increased as a result of the gravitational force and the cell was forced further towards the tip of the capillary, changing both its shape and the volumein the process. The pressure was increased in small steps and an image was made of the deformed cell at each stage. These images were analyzed using digital image analysis in order to determine the shear and compression modulus of a single cell. In using this method a few important assumptions were made, namely that there was no friction between the cell and the wall, that the capillary walls were straight at the tip region, that the cell was mechanically isotropic and that the mechanical response was purely elastic.

An experiment was performed where both the viability and morphology values of cells were measured. Cells were exposed to PBS and culture medium solutions in BSA coated and uncoated environments at room temperature for approximately one hour. In this experiment only very small differences were found between the viability percentages of all conditions and all percentages were relatively high. When looking at the determined cell diameters with both the nucleocounter and with an image analyis, there were only small differences visible when comparing the diameters within each analysis method separately. When the obtained diameters between the two analysis methods were compared, a relatively big difference was found because of another way of cell diameter determination. Finally it was concluded that both BSA coated and uncoated environments in combination with PBS or medium had no remarkable influence on the cell behavior within a one hour timeframe.

Only a small amount of experiments was performed in an appropriate way. The cause is related to problems with air bubbles, because of the adherent cell behaviors of both cell lines where cells were attached to each other (or to the walls) and because of clogging of the capillary tip as a result of (damaged) cells or dirt. During the analysis multiple strain definitions were tried in the longitudinal direction, i.e. definitions based on to the total cell length, the middle part of the cell or an average value of both of these. An attempt was made to image at higher magnifications in order to improve the quality of the images. However, this yielded insufficient contrast in the images and the decision was made to keep using a lower magnification objective.

A time dependency control experiment was performed where the cell was brought to a deformed state with small pressure steps and thus exposed to a fixed pressure for a longer time without changing any experimental conditions. This resulted in a decrease of the strain difference and volume and an increase of the pressure difference over time while the external

pressure was fixed. Reasons for this can be an "active" behavior of the cell where the cell is moving actively towards the capillary tip or because of evaporation of the liquid in the fluid reservoir around the capillary tip which results in an increasing height difference. Another explanation could be that the cell actively reorganizes its cytoskeletal structure during the experiment leading to a plastic-like mechanical response. During a second control experiment the pressure was not only increased but subsequently also decreased with small steps to investigate the elastic recovery behavior of the cell. It was observed that when the pressure was set back to zero, the cell was still deformed significantly. This indicates that cell adhesion and friction are present during the measurement and that the mechanical response of the cell is not purely elastic, with some degree of plastic deformation taking place. However, by adding a negative pressure, the cell was disconnected from the walls, and dependent on the amount of deformation, the cell was either returned to its original shape or was significantly deformed indicating plastic deformation. This behavior indicates that the mechanical response of the cells was indeed elastic, with plastic deformation occuring only at larger strain deformations.

For the shear and compression modulus a strain stiffening behavior was visible for the MDA-MB-231 cell line which resulted in a lower modulus value for small deformations and low pressures, and a higher modulus value for the larger deformations and higher pressures. For the MCF-7 cell line no significant strain sitiffening was observed and thus only one single modulus value was determined. Notably, the MCF-7 cells deformed into a tapered shape at much lower pressure values compared to the MDA-MB-231 cell line. The shear and compression modulus were higher for the strain definitions related to the total cell length and it was visible that excluding a single measurement from the total set, had a big influence on the final average moduli results. For the MDA-MB-231 cell line elastic moduli values were obtained between 290,7 Pa and 894,9 Pa for the small deformations which were comparable with literature, and small pressures and between 445,0 [pa] and 1137,2 [Pa] for larger deformations and larger pressures. For the MCF-7 cell line elastic moduli values of 14,5 Pa and 34,8 Pa were obtained. These moduli values were very low and can be trusted with more certainty when more measurements are done using multiple tip diameters.

Finally it can be concluded that it was possible to use the capillary micromechanics method to determine the mechanical properties of adherent cell types. However, the method is relatively time consuming and relies on idealized assumptions that do not completely agree with the real situation. However, multiple potential sources of error have to be carefully taken into account in order to obtain meaningful data.

7 Recommendations

In this investigation a start was made to quantitatively determine the mechanical properties of the MDA-MB-231 and MCF-7 cell lines. For a further investigation a few recommendations can be followed and improvements can be made.

It is yet unknown at which critical strain the cell from a specific cell line moves from the elastic to the plastic region. By doing an experiment where every time the pressure is increased with two steps and after making an image is decreased with one step, it could be directly observed at which point the cell is no longer moving back to the previous location. When the pressure and deformation range where the cell is still in its elastic region is known, this can be used for more accurate capillary micromechnics cell measurements.

During a measurement, for example the measurement described above, a cell tracker green (CTG) staining could be used. In combination with a fluorescence microscope the living cells will have a green color and in this way it can be checked if a living cell is measured or not.

In the Matlab code used for the analysis of the images, the assumption was made that there is no friction force between the deforming cell and the capillary walls. It is recommended to determine the friction force between the cells and a BSA coated glass wall with the use of a separate experiment and to implement the friction force results in the Matlab code for a more accurate calculation. This information could potentially also be obtained by performing separate capillary micromechnics measurements using capillaries with different taper angles.

In this investigation only small pressures were applied to the MCF-7 cell line, for a further investigation it can be interesting to see if this cell line also exhibits a strain stiffening behavior at higher deformations. Also other cell lines can be measured and compared, like the CAMA-1 cell line which was also used during the earlier appointed invastion investigation of H. Eslami Amirabadi et al[22].

The results given in this investigation can be made more accurate by carrying out more measurements on cells and by using an objective, microscope and camera combination which is able to make images with a higher magnification and a higher contrast. In this way the point selection on the cells in the capillary will be more accurate which results in more reliable values for the shear and the compression modulus.

The obtained modulus values can be used for the validation of new or improved cell measurement devices like the constriction based microfluidic chip which is designed in the thesis of R. Henderikx[7].

References

[1] ASU, Arizona State University, Jamerson Gardner. "*How many types of cells are in the human body?*". Site visited on March 23, 2018. https://askabiologist.asu.edu/questions/how-many-types-cells-are-human-body

[2] PMC, US National Library of Medicine, National Institutes of Health. Richard Mayeux. "*Biomarkers: Potential Uses and Limitations*". April, 2004. NeuroRx 1(2): 182-188.

[3] HIH, National cancer institute. "*Prostate Specific Antigen (PSA) Test*". Site visited on March 23, 2018. https://www.cancer.gov/types/prostate/psa-fact-sheet

[4] Donald Ingber. "*Mechanobiology and diseases of mechanotransduction*". June 8, 2009. Journal, Annals of Medicine. Volume 35, 2003 - issue 8, P 564-577.

[5] World Journal of Mechanics. Department of Mathematics, Indian Institute of Technology Roorkee. Vinod Kumar Katiyar and Demeke Fisseha. "*Analysis of mechanical behavior of red blood cell membrane with malaria infection*". Vol. 1 No. 3, 2011.

[6] PMC, US National library of medicine, National institutes of health. Wan Whi Low and Wan Abu Bakar Wan Abas. "*Benchtop Technologies for Circulating Tumor Cells Separation Based on Biophysical Properties.*" April 21, 2015.

[7] R.J.M. Henderikx, Technical University of Eindhoven. "*Microfluidic device to characterize the effect of chemical agents on mechanical properties of cells*". Master thesis. Eindhoven, July 2016.

[8] Trustech, innovation technology. "*MEMS, BioMEMS and Lab on Chip. Micro & Nano Technology based devices of growing importance in our society.*" Site visited on march 26, 2018. http://www.trustech.it/mems-biomems-and-lab-on-chip/.

[9] Ravetto, A. TU/e, University of Technology Eindhoven. "*Microfluidic devices for mechanical characterization and manipulation of monocytes.*" Master thesis April 7, 2015. p 51.

[10] Yu Chang Kim, Joo H. Kang, Sang-Jin Park, Eui-Soo Yoon, Je-kyun Park. "*Microfluidic biomechanical device for compressive cell stimulation and lysis*". December 12, 2007. Sensors and Actuators: Chemical, Volume 128, Issue 1, P 108-116.

[11] Hesam Babahosseini, Vaishnavi Srinivasaraghavan, Zongmin Zhao, Frank Gillam, Elizabeth Childress, Jeannine S. Strobl, Webster L. Santos, Chenning Zhang, Masoud Agah. "*The impact of sphingosine kinase inhibitor-loaded nanoparticles on bioelectrical and biomechancal properties of cancer cells.*" Jan 7, 2015. Lab Chip, 16(1): 188-198.

[12] BuckLab, Cellular Machines. "*Dual-Beam laser traps, optical stretcher, optical cell rotator.*" Site visited on March 26, 2018. https://gucklab.com/?page_id=135

[13] M. Meiling Guo and H.M. Hans Wyss. "*Micromechanics of soft particles.*" Macromelecular Materials and Engineering v296 n3-4 p 223-229. 2011.

[14] Shang-You Tee, Andreas Bausch and Paul A Janmey. US National Library of Medicine, National Institutes of Health. "*The mechanical cell.*" Curr Biol. September 15, 2009. 19(17) R745-R748. Site viewed at March 20, 2018. https://www.ncbi.nlm.nih.gov/pmc/articles/PMC2888099/

[15] Pablo Fernandez and Albrecht Ott, Physikalisches Institut, Universitat Bayreuth. "*Single cell mechanics: stress stiffening and kinematic hardening*". January 29, 2018. Site visited on May 20, 2018. https://arxiv.org/pdf/0706.3883.pdf

[16] Scitable, by nature education. "*Microtubes and filaments.*" Site visited at April 1, 2018. https://www.nature.com/scitable/topicpage/microtubules-and-filaments-14052932

[17] Virtual eUniversity. "*E-Book 02 - The cytoplasm and cellular organelles, The Cytoskeleton.*" Site visited on April 1, 2018. https://virtualuniversity.in/mod/book/tool/print/index.php?id=228&chapterid=683

[18] Welkescience. "*Microfilaments.* Site visited on April 1, 2018. https://welkescience.wikispaces.com/Microfilaments

[19] Presentation of Jasper Jacobs. "*De wondere wereld van de cel.*" Slide 20 of 27. Site visited on May 4, 2018. http://slideplayer.nl/slide/2086854/

[20] Jelle J.F. Sleeboom, Hossein Eslami Amirabadi, Poornima Nair, Cecilia M. Sahlgren and Jaap M.J. den Toonder. "*metastasis in context: modeling the tumor microenvironment with cancer-on-a-chip approaches.*" Disease models and mechanisms 11. 2018.

[21] H. Eslami Amirabadi, S. SahebAli, J.P. Frimat, R. Luttge and J.M.J. den Toonder. "*A novel method to understand tumor cell invasion: integrating extracellular matrix mimicking layers in microfluidic chips by "selective curing"*." 2017

[22] H. Eslami Amirabadi, M. Tuerlings, S. SahebAli, R. Luttge, C.C. van Donkelaar, J. Martens and J.M.J. den Toonder. "*Characterizing the invasion of different breast cancer cell lines with distinct E-cadherin status in 3D using a microfluidic system.*" Not officially published yet.

[23] ECACC, European Collection of Authenticated Cell Cultures. "*Cell line profile MDA-MB-231 (ECACC catalogue no. 92020424).*" June 2017. Site visited on December 12, 2017. https://www.phe-culturecollections.org.uk/media/133182/mda-mb-231-cell-line-profile.pdf

[24] Sigma-Aldrich. "*MCF7 cell line human, from human breast(adenocarcinoma)*". Site visited at April 5, 2018. https://www.sigmaaldrich.com/catalog/product/sigma/cb_86012803?lang=en&region=NL&gclid=EAIaIQobChMImaee4qWj2gIVRTPTCh06CghyEAAYASAAEgK93vD_BwE

[25] Xiaofeng Dai, Hongye Cheng, Zhonghu Bai and Jia Li. "*Breast cancer cell line classification and its relevance with breast tumor subtyping.*" Journal of Cancer. 2017. 8(16): 3131-3141. September 12, 2017.

[26] Thermofisher scientifuc. "*RPMI 1640 medium, GlutaMAX Supplement.*" Site visited on December 12, 2017. https://www.thermofisher.com/order/catalog/product/61870010.

[27] Hans M. Wyss, Thomas Franke, Elisa Melde, David A. Weitz. "*Capillary micromechanics: Measuring the elasticity of microscopic soft objects.*" August 9, 2010. Soft Matter journal, Issue 18, 4550-4555.

[28] Agnese Ravetto, Hans M. Wyss, Patrick D. Anderson, Jaap M.J. den Toonder, Carlijn V.C. Bouten. "*Monocytic Cells Become Less Compressible but More Deformable upon Activation.*" March 27, 2014. PLoS ONE vol. 9, nr. 3, p3.

[29] Wikipedia, The Free Encyclopedia. "*Elastic modulus, elastic moduli for homogeneous isotropic materials.*" Site visited on March 19, 2018. https://en.wikipedia.org/wiki/Elastic_modulus

[30] World Precision Instruments, Instrumenting Scientific Ideas. "*Standard Glass Capillaries, Single-Barrel Standard Borosilicate Glass Tubing Options.*" Site visited on March 1, 2018. https://www.wpiinc.com/products/top-products/make-selection-standard-glass-capillaries/

[31] Johanna Marina Jacoba Rebel , University of Rotterdam. "*Tumour cell expansion in bladder epithelium.*" Page 54. Site visited on March 3, 2018. file:///D:/Downloads/950419_REBEL,%20Johanna%20Marina%20Jacoba.pdf.

[32] Zeiss, objectiv assistant. Site visited on May 20, 2018. https://www.microshop.zeiss.com/index.php?s=125195398537705&l=en&p=us&f=o&a=v&m=s&id=420351-9910-000

[33] Medicago, your trusted partner in biotech. "*Smartbuffers, Phosphate Buffered Saline (PBS), pH 7.4 and 7.2.*" Site visited on March 20, 2018. http://www.medicago.se/sites/default/files/pdf/productsheets/PBS_Buffer_v._01.pdf

[34] Zongbin Liu, Yeonju Lee, Joon hee Jang, Ying Li, Xin Han, Kenji Yokoi, Mauro Ferrari, Ledu Zhou and Lidong Qin. "*Microfluidic cytometric analysis of cancer cell transportability and invasiveness.*" Scientific Reports v5 n1 September 25, 2015.

[35] Khanacademy. "*Phases of the cell cycle.*" Site visited on April 19, 2018. https://www.khanacademy.org/science/biology/cellular-molecular-biology/mitosis/a/cell-cycle-phases

[36] Maxim E. Dokukin, Natalia V. Guz and Igor Sokolov. "*Mechanical properties of cancer cells depend on number of passages: Atomic force microscopy indentation study.*" June 19, 2017. The Japan Society of Applied Physics, Volume 56, Number 8S1, 08LB01-08LB01.

[37] Abcam, discover more. "*Cell culture guidelines.*" Site visited on May 5, 2018. http://www.abcam.com/ps/pdf/protocols/cell_culture.pdf

[38] Cemometec. "*Eliminate human bias in cell counting, Using the Via1-cassette*". Site visited on March 22, 2018. https://chemometec.com/via1-cassette-page/

[39] ThermoFisher scientific. "*Acridine orange*". Site visited on March 22, 2018. https://www.thermofisher.com/order/catalog/product/A1301

[40] ThermoFisher scientific. "*DAPI (4', 6-Daimidino-2-Phenylindole, Dihydrochloride)*". Site visited on March 22, 2018. https://www.thermofisher.com/order/catalog/product/D1306

[41] L. Graziano and L. Preziosi, Polytechnic of Turin, Department of Mathematics. "*Mechanics in Tumor Growth.*". Site visited on April 25, 2018. http://calvino.polito.it/~preziosi/pubs/GP.pdf

[42] Elise A. Corbin, Fang Kong, Chwee Teck Lim, William P. King and Rashid Bashir. Royal society of chemistry. "*Biophysical properties of human breast cancer cells measured using silicon MEMS resonators and atomic force microscopy.*" Lab Chip, 2005, 15, 839.

[43] Sutter Instruments. "*P-97 Flaming/Brown Micropipette Puller, Operation Manual.*" Rev 2.43 - INT (20161118), page 4.

[44] ThermoFisher Scientific. "*EVO FL Imaging System, catalog number: AMF4300*". `https://www.thermofisher.com/order/catalog/product/AMF4300`. Site visited on November 7, 2017.

8 Appendix A: measurement devices

Within this appendix an overview is given of the used devices in combination with the device specifications based on specifications from manufacturers and own observations.

Table 8.1: *Flaming/Brown micropipette puller model P-97* [43]

Heat range	0 - 999
Pull range	0 - 255
Velocity range	0 - 255
Time range	0 - 255

Table 8.2: *Micro Forge MF-900*[?]

Heater stages	X, Y and Z
Pipette holder stages	X and Z
Objective lenses	5x and 10x
Eyepiece magnification	10x
Capillary diameter	1 mm

Table 8.3: *Evos FL Imaging System AMF4300*[44].

Microscopy type	Transmitted light and fluorescent
Objectives	4x, 10x and 20x
Integrated camera	Sony ICX445 monochrome CCD
Camera resolution	1280x960 pixel resolution
Camera megapixels	1,3 megapixels

Table 8.4: *Olympus polarizing microscope BX51*

Microscopy type	Brightfield and darkfield
Objective lens magnification	50x
Numerical aperture of objective	0,80
Stages	X and y direction

Table 8.5: *Zeiss axiovert 200M*

Microscopy type	Multiple fluorescent types and transmitted light
Objective lens	EC Plan Neofluar 20x/0.50 Ph2
Stages	X, Y and Z
Extra options	Temperature control
Camera	Axiocam Hrm Zeiss

9 Appendix B: image analysis point projection steps

In figure 9.1 intermediate steps of the Matlab code are shown related to the manually selected points, the fitted lines and the point projections.

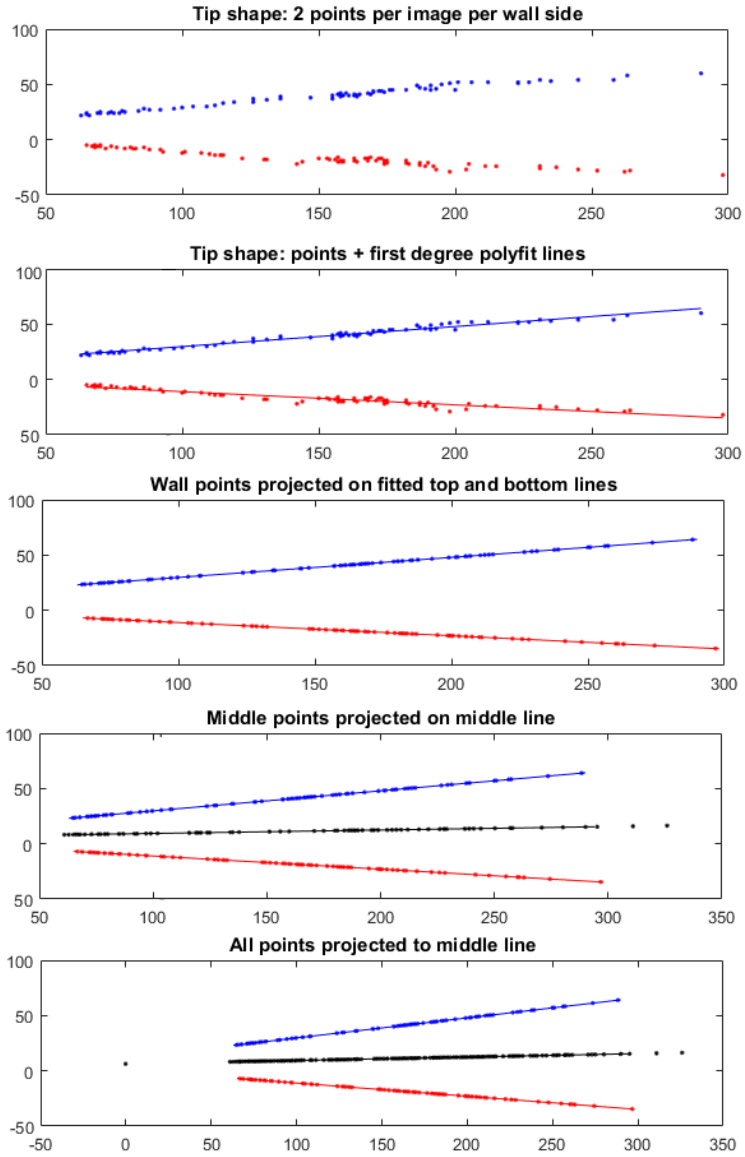

Figure 9.1: *Matlab code projection steps. Top to bottom: manual top and bottom points, line fit through manual top and bottom points, pojection of top and bottom point on line, middle line determination and projection of middle points on top of the middle line and all points projected on the middle line.*

10 Appendix C: morphology and viability analysis results

Within this appendix at first the information obtained with the VIA1 cassettes is given in table 10.1. The cell diameters [μm] are given were table 10.2 represents the uncoated situation and table 10.3 the coated situation. In each table the medium and PBS situation are given for the start situation and for the situation after one hour. Within figure 10.1 an example is given of the fluorescent markers which are present in the VIA1 cassettes to see which parts of the cell were visible and in table 10.4 these kind of images were used to determine the diameters with the use of the Matlab imdistline function.

Table 10.1: *Cell information obtained with the use of the Nucleocounter nc-200 for cells within medium or pbs for both uncoated and BSA coated situations at multiple times. The conditions were given for: M = medium, PBS, C = coated and UC = uncoated. (*1) bubble present in VIA1 cassette, results unreliable. (*2) cells flushed away while creating the 1 mL pellet mixture.*

Conditions	**Time [min]**	**Concentration [cells/mL]**	**Viability [%]**	**Average diameter [μm]**	**Theoritical cell amount**
M-UC start (*1)	0	2,27e5	99,1	15,7	-
M-UC well 1	74	1,78e5	100	15,6	-
M-UC well 2	87	1,69e5	99,6	15,5	-
M-UC well 3	98	1,91e5	99,3	15,5	-
PBS-UC start	0	7,44e5	98,6	15,8	-
PBS-UC well 1 (*2)	-	-	-	-	2,232e5
PBS-UC well 2	90	1,25e5	95,1	15,3	2,232e5
PBS-UC well 3	101	1,26e5	95,2	15,3	2,232e5
M-C start	0	1,17e6	99,1	15,0	-
M-C well 1	73	2,12e5	99,3	15,3	2,346e5
M-C well 2	81	2,35e5	98,9	15,4	2,346e5
M-C well 3	91	2,35e5	98,8	15,3	2,346e5
PBS-C start	0	1,42e6	99,1	15,0	-
PBS-C well 1	74	2,03e5	96,3	14,8	2,844e5
PBS-C well 2	81	2,25e5	89,2	15,0	2,844e5
PBS-C well 3	89	1,66e5	94,2	15,0	2,844e5

Table 10.2: *Cell diameters determined by an image analysis (imdistline function of Matlab) for cells within medium or PBS at the start and after one hour for the UNCOATED situation.*

Diameter medium before [μm]	**Diameter medium after [μm]**	**Diameter PBS before [μm]**	**Diameter PBS after [μm]**
20,2785	16,2263	17,3066	17,7101
24,9121	16,8163	17,2155	17,5192
19,6104	34,5742	21,7059	17,6971
21,0899	34,6176	22,7732	18,6950
17,5235	18,3001	15,9616	17,4021

16,2957	18,8555	16,3782	18,4693
22,0010	17,7231	17,5843	19,3197
21,3111	17,5843	18,2134	20,9944
20,1223	18,2394	18,4842	18,1483
21,3632	17,2198	18,2264	18,6169
18,9683	20,0312	27,6021	22,3871
18,6429	17,7752	29,5371	23,1767
17,7231	24,0184	17,3587	18,3218
19,3154	23,2678	16,8511	18,0225
18,3175	19,1505	20,2568	18,4477
18,8034	17,0853	19,6191	18,7253
18,2958	21,5367	17,5322	25,3807
19,9662	19,8143	15,8532	24,9035
18,9336	19,3414	20,7384	18,2568
18,7340	22,8947	20,3827	19,8881
17,7144	20,1310	18,0876	15,6883
18,3782	19,8620	19,5974	15,8141
14,5907	20,6647	16,8294	16,4259
16,8120	19,3067	15,3065	18,1266
30,8560	23,7320	29,8321	19,1505
27,5587	21,6495	27,2984	17,7275
17,1200	17,3240	19,8143	16,8120
16,8163	15,6840	19,2373	18,1526
25,0380	16,9725	20,6386	17,8272
24,5824	16,6124	19,1375	17,3760
20,0226	17,9531	23,1984	14,8423
20,6603	17,4802	22,5823	15,1460
20,6690	19,9141	16,1222	32,2877
19,4499	21,1723	16,5560	30,8908
25,2028	21,2851	16,8077	17,6580
23,9707	22,1138	15,7447	16,6211
23,3416	21,6322	17,4324	18,2394
23,7364	20,3176	17,6277	18,4954
15,8402	17,6971	14,6731	20,0529
17,5713	16,4996	13,4236	20,8035
18,3522	22,0010	21,7016	18,8945
19,9575	20,2742	21,4152	19,7058
15,1026	15,7968	18,6472	18,5214
16,3608	15,9833	18,2004	17,2459
22,5346	14,8770	18,9596	17,0723
21,3372	15,6753	21,4369	17,7275
18,2698	17,4194	19,0290	16,3955
17,8880	15,8358	19,4933	18,4997

Table 10.3: *Cell diameters determined by an image analysis (imdistline function of Matlab) for cells within medium or PBS at the start and after one hour for the COATED situation.*

Diameter medium before [μm]	**Diameter medium after [μm]**	**Diameter PBS before [μm]**	**Diameter PBS after [μm]**
23,0682	19,3891	20,4217	17,8229
20,4521	17,3196	19,6711	17,5149
16,6688	13,5147	19,1592	19,9965
15,9660	14,2870	18,0745	20,2438
18,4563	16,8944	16,0745	18,0485
17,2155	17,6754	18,4867	18,3522
13,9572	20,8382	16,6645	18,0051
13,7229	21,6929	17,2979	19,2112
19,7709	29,4937	17,3283	18,4954
18,5865	32,9602	18,3826	16,6385
20,5172	20.4955	19,3024	13,8140
20,1223	25,5803	18,6082	15,1503
21,8708	17,2025	23,3589	19,6191
20,5779	16,4996	24,0184	18,1266
15,8228	18,8511	19,1462	22,5433
16,9031	18,9770	16,6124	22,8687
17,0506	17,2025	16,1612	16,0050
16,6385	17,8923	17,9661	16,9205
15,7187	19,5757	27,3374	16,7773
15,2414	21,6061	28,8689	16,6558
21,5628	23,9577	16,8988	16,7296
20,7211	23,4587	16,7773	17,2415
28,7691	20,3740	17,8923	16,7426
26,4220	20,1310	18,3782	15,6015
16,8727	20,3480	16,0528	20,3089
16,8250	22,2135	15,2241	18,4780
20,1571	17,8142	17,0159	14,9117
19.,8143	17,9270	16,2350	13,5624
18,2611	18,9943	17,2719	15,7794
17,4671	19,0811	17,9704	15,0592
15,1113	17,7535	20.2785	18,3739
15,1286	17,6624	18,2958	17,9487
18,9249	17,4541	17,9747	15,5451
18,2437	17,9227	16,3955	15,6753
18,3132	16,1482	18,4737	19,9662
16,3738	16,3348	20,4087	21,7753
18,9553	14,7295	15,3022	18,8642
21,5237	15,3065	17,1678	17,4368
16,1699	22,4175	16,9639	16,0007
18,4693	22,0010	15,5495	16,0788
20,1484	17,9010	16,3131	17,6797
17,9964	18,5171	17,3630	18,6776

19,6234	18,9292	21,4066	17,4107
19,0160	18,3696	23,6062	16,8120
22,2396	17,5322	15,4106	17,0550
23,8796	19,5193	14,1004	17,7622
15,7360	15,8879	13,1806	17,9270
16,3174	17,0984	13,1980	19,1939

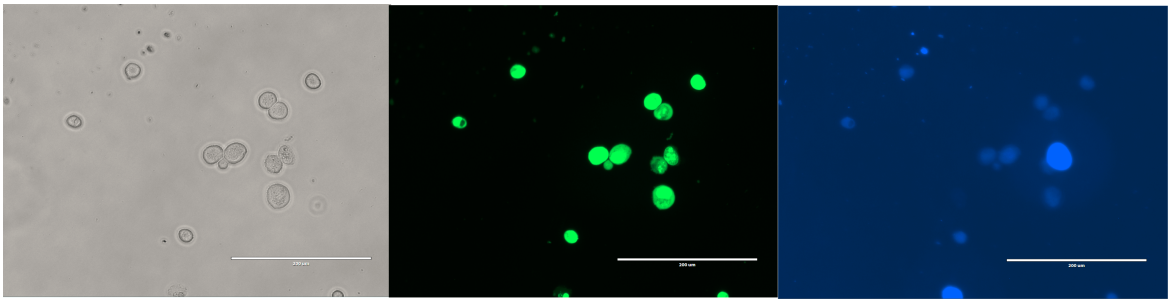

Figure 10.1: *Visible parts of cells with different fluorescent stainings (MDA-MB-231 cell type). Left: transmitted light of EVOS microscope. Middel: GFP light cube of EVOS microscope. Right: DAPI light cube of EVOS microscope.*

Table 10.4: *Cell diameters determined with the imdistline function of Matlab based on transmitted light images and acridine orange staining images.*

Cell diameter transmitted light [μm]	**Cell diameter acridine orange staining [μm]**
45,42	35,76
48,21	34,91
43,31	41,92
42,30	40,57
43,56	39,44
40,01	35,56
45,98	41,41
46,26	45,17
44,49	42,34
44,18	41,80
34,60	32,65
32,83	30,86
42,15	39,42
36,75	35,68
36,44	32,70
37,57	34,64
44,07	42,80
38,97	37,57
40,94	37,89
40,85	38,23

11 Appendix D: statistics

Within this appendix the tables are given which are based on statistical information generated with the R Commander program. Each executed test contains of an ANOVA test and a Tukey contrast test for the six cell environments.

11.1 VIA1 viability percentages

In table 11.1 the most important test statistics for a pairwise comparison of the different situations is given for the VIA1 viability percentage measurements. With the null hypotheses that all average values are equal, this hypothesis can be rejected based on the information given in table 11.1. The difference was investigated with a pairwise comparison of the means with the use of the Tukey contrast test. When a value of p from this test was higher then 0,05 there was no significant difference, else the difference was significant at a specific significance level. Looking to table 11.1, the conclusion was made that there were significant differences between the different conditions and these differences were: coated PBS and coated start situation and coated PBS and coated medium situation with 0,05 levels of significance, coated PBS and uncaoted medium situation with a 0,01 level of significance, and between the coated PBS and uncoated start situation with a 0,1 level of significance.

Table 11.1: *One way ANOVA and Tukey contrast results for the VIA1 viability percentage measurements for al situations.*

F_{ANOVA}	6,291	
p_r(>F)	0,00885	
Degrees of freedom (numerator)	5	
Degrees of freedom (denominator)	9	
Compared pairs	**t-value**	$P_r>\|t\|$
uncoated medium - uncoa-ted start	0,494	0,9951
uncoated PBS - uncoated start	-2,131	0,3496
coated start - uncoated start	0,144	1,0000
coated medium - uncoated start	0,095	1,0000
coated PBS - uncoated start	-3,544	0,0502
uncoated PBS - uncoated medium	-2,829	0,1391
coated start - uncoated medium	-0,337	0,9992
coated medium - uncaoted medium	-0,447	0,9969
coated PBS - uncoated medium	-4,515	0,0129
coated start - uncoated PBS	2,275	0,2925
coated medium - uncoated PBS	2,429	0,2397
coated PBS - uncoated PBS	-1,209	0,8214
coated medium - coated start	-0,063	1,0000
coated PBS - coated start	-3,702	0,0401
coated PBS - coated medium	-4,068	0,0240

11.2 Imdistline diameter measurements

In table 11.2 the most important test statistics for a pairwise comparison of the different situations is given for the imdistline diameter measurements. With the null hypotheses that

all average values are equal, this hypothesis can be rejected based on the information in table 11.2. Looking to table 11.2, the conclusion was made that there was only a significant difference between the coated PBS and the uncoated medium situation with a 0,05 level of significance and between the coated PBS situation and the uncoated start situation with a 0,01 level of significance. Based on this statistics only the coated PBS situation was statistically different compared to some other average values.

Table 11.2: *One way ANOVA and Tukey contrast results for the imdistline diameter measurements for all situations.*

F_{ANOVA}	3,384	
p_r(>F)	0,00528	
Degrees of freedom (numerator)	5	
Degrees of freedom (denominator)	278	
Compared pairs	**t-value**	$P_r>\|t\|$
uncoated pbs - uncoated medium	-0,830	0,96103
uncoated start - uncoated medium	0,152	0,99999
coated medium - uncoated medium	-0,536	0,99455
coated PBS - uncoated medium	-2,912	0,04271
coated start - uncoated medium	-1,986	0,34796
uncoated start - uncoated PBS	1,111	0,87469
coated medium - uncoated PBS	0,294	0,99970
coated PBS - uncoated PBS	-2,082	0,29479
coated start - uncoated PBS	-1,027	0,90690
coated medium - uncoated start	-0,771	0,97164
coated PBS - uncoated start	-3,515	0,00621
coated start - uncoated start	-2,618	0,09377
coated PBS - coated medium	-2,376	0,16431
coated start - coated medium	-1,367	0,74311
coated start - coated PBS	1,377	0,73717

11.3 VIA1 diameter measurements

In table 11.3 the most important test statistics for a pairwise comparison of the different situations is given for the VIA1 diameter measurements. With the Tukey contrast test it was visible that the most average values for the different situations were significant different at significance levels varying from 0,1 to 0,001.

Table 11.3: *One way ANOVA and Tukey contrast results for the VIA1 diameter measurements for all situations.*

F_{ANOVA}	46,2	
p_r(>F)	3,78e^{-6}	
Degrees of freedom (numerator)	5	
Degrees of freedom (denominator)	9	
Compared pairs	**t-value**	$P_r>\|t\|$
uncoated PBS - uncoated medium	-3,615	0,04546
uncoated start - uncoated medium	3,357	0,06572
coated start - uncoated medium	-8,262	<0,001
coated medium - uncoated medium	-3,464	0,05649
coated PBS - uncoated medium	-10,392	<0,001
uncoated start - uncoated PBS	6,364	0,00122
coated start - uncoated PBS	-4,243	0,01881
coated medium - uncoated PBS	0,516	0,99403
coated PBS - uncoated PBS	-5,680	0,00291
coated start - uncoated start	-10,607	<0,001
coated medium - uncoated start	-6,455	0,00112
coated PBS - uncoated start	-12,652	<0,001
coated medium - coated start	5,164	0,00550
coated PBS - coated start	-1,033	0,89469
coated PBS - coated medium	-6,928	< 0,001

12 Appendix E: experimental and analytical conditions

Within this appendix information related to the experimental setup and protocol, the strain definitions and the image quality improvement are given.

12.0.1 Experimental setup and protocol

During the build up and improvement phase of the experimental setup at first the EVOS microscope and a non digital inverted microscope were used to observe the capillary tip and the fluid flow inside this capillary. With both microscopes a flow was visible based on streamlines at the tip location and based on the movement of small particles inside the capillary (for example dirt which entered the needle during the withdrawing steps of the device preparation). During this stage of the experimental setup development it turned out to be impossible to observe the cells with the use of these microscopes and a switch was made to the Zeiss Axiovert 200M. With the use of this microscope the cells were visible inside the capillary tip, probably because of the present light cubes, contrast filters and microscopic properties. Based on the experiments a height change was determined around one centimeter, related to the fluid reservoir level at the tip, which was enough to deform the cells within the fabricated capillaries. First, a three way valve was placed between the tube of the device and the height regulating reservoir, with the idea to have a third inlet which was able to enable using hand pressurizing situations and for an easier way to remove air bubbles. Because of a big amount of cell accumulation at the edges of the valve this valve was removed and the length of the final connection tube was made as small as possible in the final setup.

12.0.2 Strain definition and image quality improvement

Within the Matlab code three different strain definitions were tried as described in section 3.7. During the analysis the decision was made to use both the total cell length for the strain in the longitudinal direction and the strain in only the middle part. For all strain definitions in the longitudinal direction the same strain definition was used for the radial direction, which was based on the radius located at the middle of the contact band. These strain definitions result in a minimal and a maximal modulus. The definition where the average strain was used, resulted in values which were almost all the average of the two other strain definitions.

When the Zeiss Axiovert 200M was chosen to use an image improvement was tried. In figure 12.1 'A' a 6,88 μm tip is visible through the PH2 Plan-Neofluar 20x/0.50 objective which resulted with the exta 1,6 function to a total magnification of 32x. It was not possible to use the objectives available on the microscope with higher magnifications because of the too small working distances for the experiment. Even when a 0,17 μm thick glass layer was used instead of the 1 mm thick layer at the bottom of the fabricated devices, the working distance was still too big. In figure 12.1 'B' a 40x magnification (64x with 1,6 function) dipping objective was used with a higher working range. This image looks out of focus, but it was not possible to image the capillary any more clearly. The higher magnification resulted in a bigger view of the capillary, but a lower contrast and based on this observation the decision was made to stay at the 20x magnification objective.

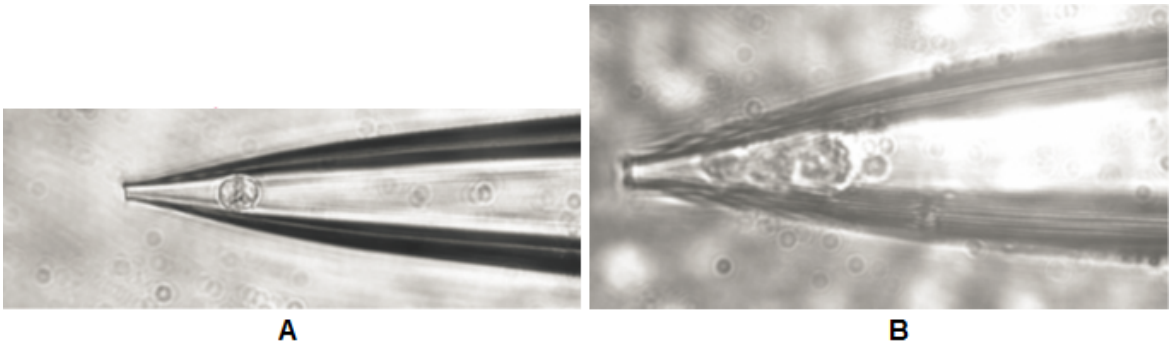

Figure 12.1: *Objective change Zeiss Axiovert 200M. Left 32x magnification on a 6,88 µm tip and right a 64x magnificatin on a 4,79 µm tip.*

13 Appendix F: shear and compression modulus graphs

In the figures below the shear and compression modulus values are given for both the MDA-MB-231 and MCF-7 measurements.

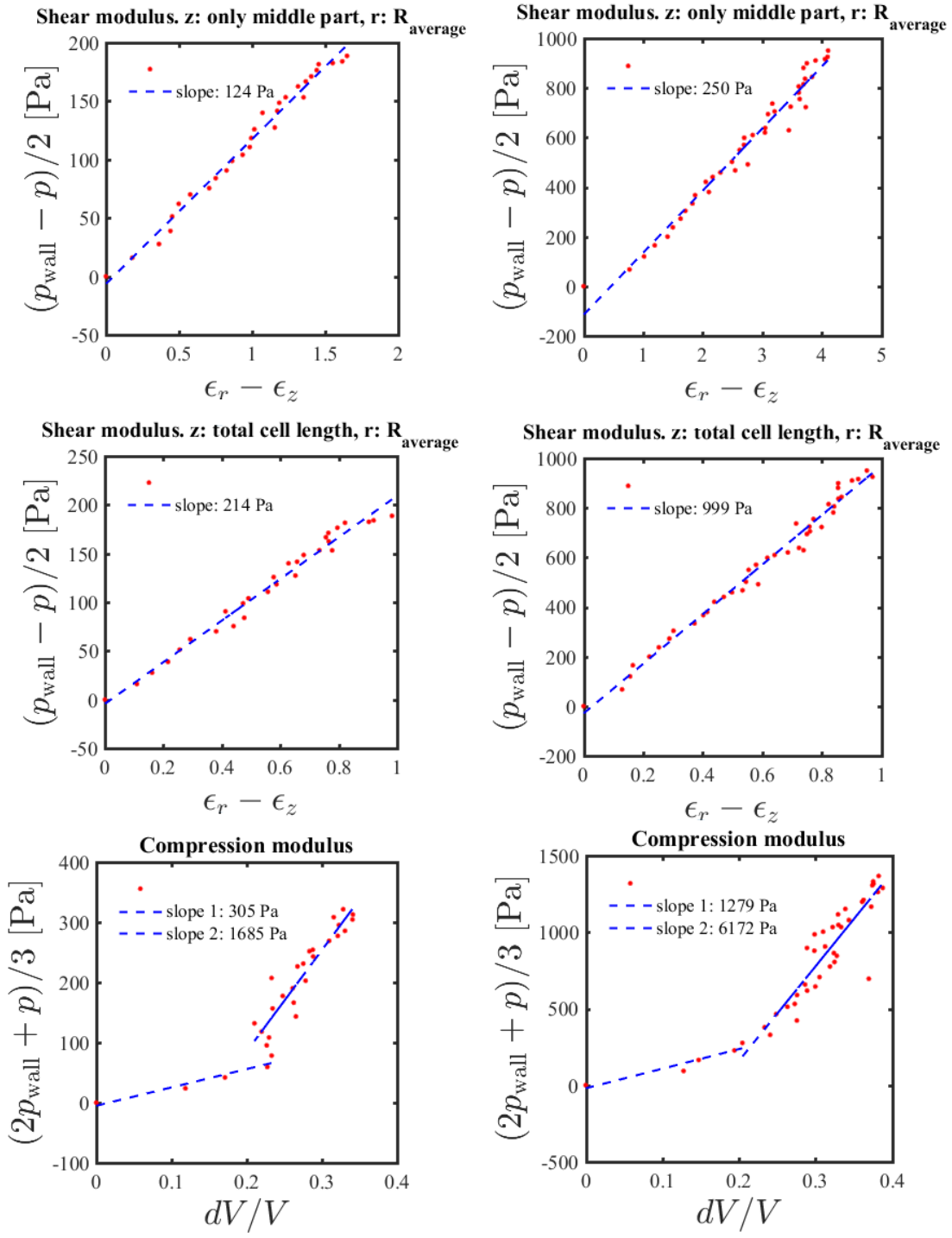

Figure 13.1: *MDA-MB-231 shear and compression modulus. Left: 6,97 µm tip diameter, 70 pa pressure. Right: 5,88 µm tip diameter, 100 Pa pressure.*

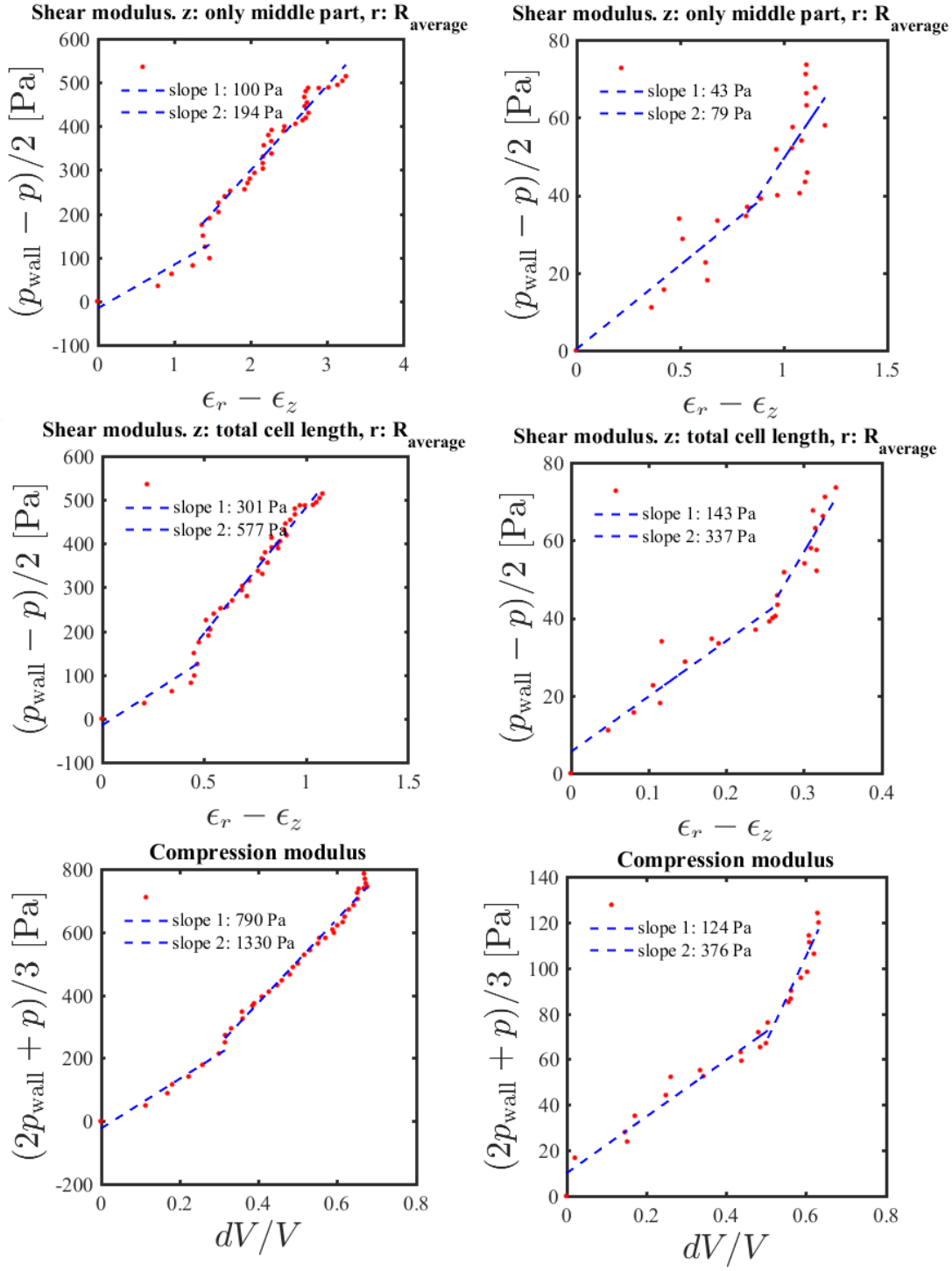

Figure 13.2: *MDA-MB-231 shear and compression modulus. Left: 5,88 µm tip diameter, 100 Pa pressure. Right: 9,07 µm tip diameter, 26 Pa pressure.*

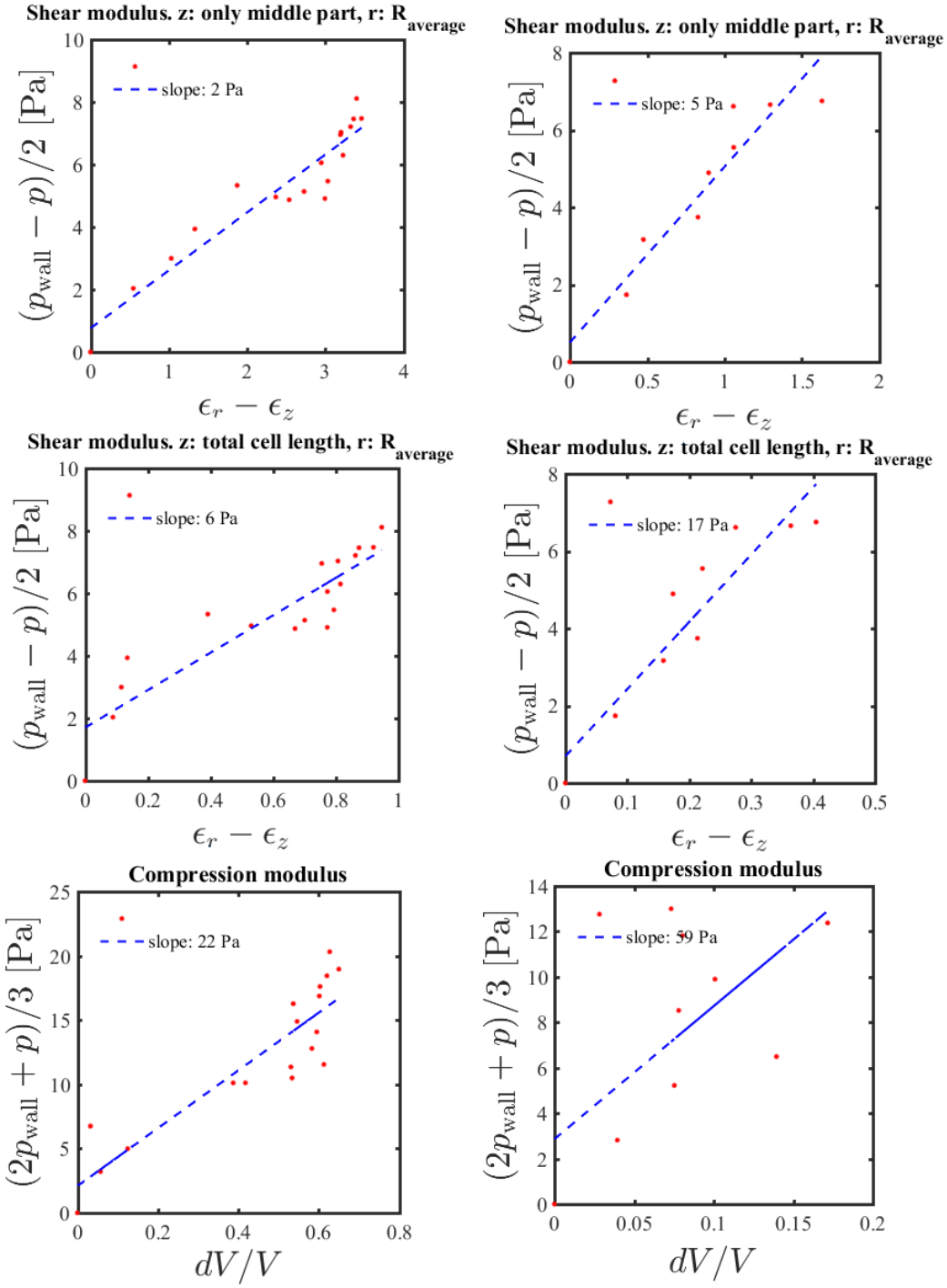

Figure 13.3: *MCF-7 shear and compression modulus. Left: 7,22 µm tip diameter, 8,5 Pa pressure. Right: 7,22 µ tip diameter, 9,5 Pa.*

14 Appendix G: band length and average radius, error analysis

Within this appendix the minimal and maximal band length and the minimal and maximal average radius of all cell measurements are given which are used for the calculation of the volumetric error percentage as a result of the manual point selection during the image analysis.

Table 14.1: *Volumetric error dimensions. Minimal and maximal band length and minimal and maximal average radius for all used measurements in pixels.*

$L_{band,min}$	$L_{band,max}$	$R_{average,min}$	$R_{average,max}$
33,9	93,1	22,1	46,8
39,1	87,5	15,7	26,5
24,6	89,3	14,6	37,4
15,9	74,1	15,0	27,5
31,3	53,1	21,2	36,3
34,1	76,6	16,0	29,2
26,9	105,0	17,2	38,7
40,7	98,9	29,1	37,0

15 Appendix H: Matlab code

Within this section the Matlab code is given which is used for the calculations of the compression and the shear modulus based on the pressure and geometry text files.

```
%%%%%%%%%%%%%%%%%%%%%%%%%%%%%%%%%%%%%%%%%%%%%%%%%%%%%%%%%%%%
%  Rewritten Matlab script capillary micromechanics.       %
%  Thomas Doomen                                           %
%  05-04-2018                                              %
%  Based on the already existing script of H.M. Wyss.     %
%%%%%%%%%%%%%%%%%%%%%%%%%%%%%%%%%%%%%%%%%%%%%%%%%%%%%%%%%%%%

%% Prepare file
clear all
close all
clc

%% Load .txt files of pressure and geometry
[FileName,PathName]=uigetfile('pressurecel7.txt','Select the Pressure file (mm H2O)..');
cd ([PathName,'\']);
p_data_file=([PathName,'\',FileName]);

[FileName,PathName]=uigetfile('geometrycel7.txt','Select the ball geometry data file..');
cd ([PathName,'\']);
geometry_data_file=([PathName,'\',FileName]);

%% Read datafiles
geometry_data = importdata(geometry_data_file); %Import geometry datafile
colheaders = genvarname(geometry_data.colheaders);
point=NaN; x=NaN; y=NaN; slice=NaN; color=NaN;  %Introduce parameters without value
point=geometry_data.data(:,1);                  %Point number at specific image
x=geometry_data.data(:,2);                      %X value in pixels
y=geometry_data.data(:,3);                      %Y value in pixels
slice=geometry_data.data(:,4);                  %Image number
color=geometry_data.data(:,5);                  %Color value of ImageJ selection points

p_data = importdata(p_data_file);               %Import pressure datafile
colheaders = genvarname(p_data.colheaders);
frame=NaN; height=NaN;                          %Introduce parameters without value
frame=p_data.data(:,1);                         %Image number
height=p_data.data(:,2);                        %Height related to image number in [mm]

%% Spicify point and image numbers
n_points_total = length(x);                     %Number of selected ImageJ points
n_images_total = max(slice);                    %Number of images
n_points_per_image_total = max(point)+1;        %Number of points per image

%Load all the image numbers which you want to use: for example 1:41, the maximum number is given in the commentbar
inputvalue1 = inputdlg(['Which images must be used? Input by space separated numbers (1 2 3), ranges(1:9) or combinations of these. Maximum number is ' num2str(n_images_total)],...
```

```
45              'Sample', [1 100]);
46
47 images_chosen = str2num(inputvalue1{1});          %Create vector of chosen
       image number values
48 N_images = length(images_chosen);                 %Number of chosen images
49
50 %% Top and bottom line fit
51 i=1;                                               %Introduce variables
52 k=1;
53 x_coords=0; y_coords=0;
54 x_coords2=0; y_coords2=0;
55
56 for j = 1:N_images                                 %Number of chosen
       images
57     n = images_chosen(j);                          %Select value number
           'j' from the chosen images vector
58
59     % Top line points
60     x0=x(7*n-6);                                   %X coordinate
           reference
61     y0=y(7*n-6);                                   %Y coordinate
           reference
62     x_coords(i)=x(7*n-5)-x0; y_coords(i)=y(7*n-5)-y0;   %Relative left top
           point
63     i=i+1;
64     x_coords(i)=x(7*n-4)-x0; y_coords(i)=y(7*n-4)-y0;   %Relative right top
           point
65     i=i+1;
66
67     %Linear fit top (degree 1)
68     p_top=polyfit(x_coords,y_coords,1);    %First order polyfit through
           x_coords and y_coords
69     a_top_fit=p_top(2);                    %y=a+b*x = p(2)+p(1)x
70     b_top_fit=p_top(1);
71
72     % Bottom line points
73     x_coords2(k)=x(7*n-3)-x0; y_coords2(k)=y(7*n-3)-y0; %Relative left bottom
           point
74     k=k+1;
75     x_coords2(k)=x(7*n-2)-x0; y_coords2(k)=y(7*n-2)-y0; %Relative right
           bottom point
76     k=k+1;
77
78     %Linear fit bottom (degree 1)
79     p_bot=polyfit(x_coords2,y_coords2,1);    %First order polyfit through
           x_coords and y_coords
80     a_bot_fit=p_bot(2);                      %y=a+b*x = p(2)+p(1)x
81     b_bot_fit=p_bot(1);
82 end
83
84 %% Subfigures top and bottom points and fitted lines of walls
85 figure(1)
86 subplot(3,2,1)
87 plot(x_coords, y_coords, 'r.')
88 hold on
89 plot(x_coords2, y_coords2, 'b.')
90 title('Tip shape: 2 points per image per wall side')
91 subplot(3,2,2)
92 p_topfit = polyval(p_top,x_coords);
93 p_botfit = polyval(p_bot,x_coords2);
```

```
plot(x_coords, y_coords, 'r.')
hold on
plot(x_coords2, y_coords2, 'b.')
hold on
plot(x_coords,p_topfit,'r-')
hold on
plot(x_coords2, p_botfit, 'b-')
title('Tip shape: points + first degree polyfit lines')

%% Angle between top and bottom line with the centerline
alpha = abs(b_top_fit+b_bot_fit)/2; %b values are slopes of both lines, abs
    to get positive value, /2 for single angle (average).

%% Point coordinates and middle line

for j = 1:N_images                                          %Number of chosen
    images
    n = images_chosen(j);                                   %Select value number
        'j' from the chosen images vector
    %Get positions relative to reference point:
    p1.x=x(7*n-5)-x0;p1.y=y(7*n-5)-y0;  %Cell point 1 = left top
    p2.x=x(7*n-4)-x0;p2.y=y(7*n-4)-y0;  %Cell point 2 = right top
    p3.x=x(7*n-3)-x0;p3.y=y(7*n-3)-y0;  %Cell point 3 = left bottom
    p4.x=x(7*n-2)-x0;p4.y=y(7*n-2)-y0;  %Cell point 4 = right bottom
    p5.x=x(7*n-1)-x0;p5.y=y(7*n-1)-y0;  %Cell point 5 = left middle
    p6.x=x(7*n)-x0;p6.y=y(7*n)-y0;      %Cell point 6 = right middle

    %Middle line
    a_mid_fit=(a_top_fit+a_bot_fit)/2;              %Startpoint of midddle
        line
    b_mid_fit=(b_top_fit+b_bot_fit)/2;              %Slope of middle line

    %Project manual points onto top, bottom and middle lines
    [p1.x,p1.y]=projection(a_top_fit,b_top_fit, p1.x,p1.y);
    [p2.x,p2.y]=projection(a_top_fit,b_top_fit, p2.x,p2.y);
    [p3.x,p3.y]=projection(a_bot_fit,b_bot_fit, p3.x,p3.y);
    [p4.x,p4.y]=projection(a_bot_fit,b_bot_fit, p4.x,p4.y);
    [p5.x,p5.y]=projection(a_mid_fit,b_mid_fit, p5.x,p5.y);
    [p6.x,p6.y]=projection(a_mid_fit,b_mid_fit, p6.x,p6.y);

    xProjectiontop = [p1.x p2.x]; yProjectiontop = [p1.y p2.y];
    xProjectionbot = [p3.x p4.x]; yProjectionbot = [p3.y p4.y];
    xProjectionmid = [p5.x p6.x]; yProjectionmid = [p5.y p6.y];

    %Plot of middle line and projected points
    subplot(3,2,3)
    plot(x_coords,p_topfit,'r-')
    hold on
    plot(x_coords2, p_botfit, 'b-')
    hold on
    plot(xProjectiontop, yProjectiontop, 'r.')
    hold on
    plot(xProjectionbot, yProjectionbot, 'b.')
    title('Wall points projected on fitted top and bottom lines')
    subplot(3,2,4)
    plot(x_coords,p_topfit,'r-')
    hold on
    plot(x_coords2, p_botfit, 'b-')
    hold on
    plot(xProjectiontop, yProjectiontop, 'r.')
```

```
150     hold on
151     plot(xProjectionbot, yProjectionbot, 'b.')
152     hold on
153     plot(xProjectionmid, yProjectionmid, 'k.')
154     hold on
155     plot(((x_coords+x_coords2)./2), a_mid_fit+b_mid_fit*((x_coords+x_coords2)
            ./2), 'k')
156     title('Middle points projected on middle line')
157
158     %Projections of all points related to middle line
159     [p0mid.x,p0mid.y]=projection(a_mid_fit,b_mid_fit,0,0);
160     [p1mid.x,p1mid.y]=projection(a_mid_fit,b_mid_fit,p1.x,p1.y);
161     [p2mid.x,p2mid.y]=projection(a_mid_fit,b_mid_fit,p2.x,p2.y);
162     [p3mid.x,p3mid.y]=projection(a_mid_fit,b_mid_fit,p3.x,p3.y);
163     [p4mid.x,p4mid.y]=projection(a_mid_fit,b_mid_fit,p4.x,p4.y);
164     [p5mid.x,p5mid.y]=projection(a_mid_fit,b_mid_fit,p5.x,p5.y);
165     [p6mid.x,p6mid.y]=projection(a_mid_fit,b_mid_fit,p6.x,p6.y);
166
167     pxmid = [p0mid.x p1mid.x p2mid.x p3mid.x p4mid.x p5mid.x p6mid.x];
168     pymid = [p0mid.y p1mid.y p2mid.y p3mid.y p4mid.y p5mid.y p6mid.y];
169
170     %Plot of all points projected on middle line
171     subplot(3,2,5)
172     plot(x_coords,p_topfit,'r-')
173     hold on
174     plot(x_coords2, p_botfit, 'b-')
175     hold on
176     plot(xProjectiontop, yProjectiontop, 'r.')
177     hold on
178     plot(xProjectionbot, yProjectionbot, 'b.')
179     hold on
180     plot(xProjectionmid, yProjectionmid, 'k.')
181     hold on
182     plot(pxmid, pymid, 'k.')
183     hold on
184     plot(((x_coords+x_coords2)./2), a_mid_fit+b_mid_fit*((x_coords+x_coords2)
            ./2), 'k')
185     hold on
186     title('All points projected to middle line')
187
188     %Distance of points on the middle line to the reference point on the
189     %middle line.
190     d1=dist_2D(p1mid.x,p1mid.y,p0mid.x,p0mid.y);
191     d2=dist_2D(p2mid.x,p2mid.y,p0mid.x,p0mid.y);
192     d3=dist_2D(p3mid.x,p3mid.y,p0mid.x,p0mid.y);
193     d4=dist_2D(p4mid.x,p4mid.y,p0mid.x,p0mid.y);
194     d5=dist_2D(p5mid.x,p5mid.y,p0mid.x,p0mid.y);
195     d6=dist_2D(p6mid.x,p6mid.y,p0mid.x,p0mid.y);
196
197     %Contact area between cell and capillary wall and volume determination
198     d_mid_front=(d1+d3)/2;                          %Middle line distance
            front points to reference (average)
199     d_mid_back=(d2+d4)/2;                           %Middle line distance
            back points to reference (average)
200     L_band(j)=d_mid_back-d_mid_front;                %Contact length
            longitudinal direction (on middle line)
201     L_band_2= d6-d5;                                %Total cell lenght over
             middle line for second strain graph
202     L_band_average = (L_band(j)+L_band_2)/2;
203     W_band_top=dist_2D(p1.x, p1.y, p2.x, p2.y);     %Contact length based
```

```
    on top points.
204     W_band_bottom=dist_2D(p3.x, p3.y, p4.x, p4.y);     %Contact length based
        on bottom points.
205     W_band=(W_band_top+W_band_bottom)/2;               %Average contact length
         top and bottom.
206     R_front_1=dist_2D(p1.x, p1.y, p1mid.x, p1mid.y);   %Front radius based on
        point 1.
207     R_front_2=dist_2D(p3.x, p3.y, p3mid.x, p3mid.y);   %Front radius based on
        point 3.
208     R_front=(R_front_1+R_front_2)/2;                   %Average front radius.
209     R_back_1=dist_2D(p2.x, p2.y, p2mid.x, p2mid.y);    %Back radius based on
        point 2.
210     R_back_2=dist_2D(p4.x, p4.y, p4mid.x, p4mid.y);    %Back radius based on
        point 4.
211     R_back=(R_back_1+R_back_2)/2;                      %Average back radius.
212
213     A_band(j)=pi*(R_front+R_back)*sqrt((R_front-R_back)^2+ L_band(j)^2);     %
        Lateral surface area
214     V_band=(1/3)*pi*L_band(j)*(R_front^2+R_back^2+(R_front*R_back));         %
        Volume of band
215     L_front_cap=d_mid_front-d5;                                              %
        Front cap length on middle line
216     L_back_cap=d6-d_mid_back;                                                %
        Back cap length on middle line
217     V_front_cap=((pi*L_front_cap)/6)*(3*R_front^2+L_front_cap^2);            %
        Volume spherical front cap
218     V_back_cap=((pi*L_back_cap)/6)*(3*R_back^2+L_back_cap^2);                %
        Volume spherical back cap
219     V_total(j) = V_band+V_front_cap+V_back_cap;                              %
        Total volume of cell
220
221     R_band_average(j)=(R_front+R_back)/2;               %Average band radius
222     A_band_middle=pi*R_band_average(j)^2;               %Area of average band
223
224     %External pressure and wall pressure
225     p_external(j)=height(n)*10;                             %External pressure
226     External_force(j)=p_external(j)*(pi*R_back^2);          %External force on
         back area
227     Wall_force(j)=External_force(j)/(sin(alpha));           %Wall force (
        Fwall_long = Fp)
228     p_wall(j)=Wall_force(j)/A_band(j);                      %Wall pressure
229     P_difference=p_wall(j)-p_external(j);                   %Pressure
        difference
230     p_difference(j)=P_difference;
231     p_average(j)=(2*p_wall(j)+p_external(j))/3;         %Average pressure 2D:
        two contributions of wall and one from external pressure
232
233     %Strains
234     if j==1     %First image = no pressure on cell
235         R_0=(3*V_total(j)/4/pi)^(1/3);          %Radius of sphere with total
            cell volume
236         R_band_strain=0;                        %Zero strain at start
237         R_band0=R_band_average(j);              %R_band at start is avarage
            band
238         L_band_strain = 0;
239         V_strain = 0;
240         L_band0=L_band(j);                      %Band length at start (middle
             part).
241         L_band0_2=L_band_2;                     %Band length at start (total
            cell length)
```

```
242         L_band0_3=L_band_average;                %Band length average value
243         e_r=0;                                   %Strain in radial and
                longitudinal direction equal to zero
244         e_z=0;
245         V0=V_total(j);
246
247     else
248         R_band_strain(j)=(R_band0-R_band_average(j))/R_band0;   %Strain based
                on middle part
249         L_band_strain(j)=(L_band0-L_band(j))/L_band0;
250         e_r(j)=R_band_strain(j);
251         e_z(j)=L_band_strain(j);
252         e_G_(j)=2*(e_r(j)-e_z(j));
253
254         R_band_strain_total(j) = (R_band0-R_band_average(j))/R_band0;   %
                Strain based on total cell length
255         L_band_strain_total(j) = (L_band0_2-L_band_2)/L_band0_2;
256         e_r_total(j) = R_band_strain_total(j);
257         e_z_total(j) = L_band_strain_total(j);
258         e_G_2(j) = 2*(e_r_total(j)-e_z_total(j));
259
260         R_band_strain_average(j) = (R_band0-R_band_average(j))/R_band0;  %
                Strain based on average value
261         L_band_strain_average(j) = (L_band0_3-L_band_average)/L_band0_3;
262         e_r_average = R_band_strain_average(j);
263         e_z_average = L_band_strain_average(j);
264         e_G_3(j) = 2*(e_r_average-e_z_average);
265
266         V_strain=(V0-V_total(j))/V0; %Volumetric strain
267         V_strain_(j)=V_strain;
268
269         K_(j)= (2*p_wall(j) + p_external(j))/3 / (2*e_r(j) + e_z(j));    %
                Compression modulus
270         G_(j)= (p_wall(j) - p_external(j))/2/(e_r(j) - e_z(j));          %
                Shear modulus
271     end
272 end
273
274 %Output:
275 column_names = {'       L_band        ', 'R_band_average  ', 'L_band_strain '
    , 'Total volume     ', 'p_external     ', 'p_wall       ', 'p_wall-p
         ', '  A_band     ' , 'Wall_force       ', 'External_force     ', '
    R_band_strain        ', '       e_r mid      ', 'e_z mid      ', 'e_r tot
          ', 'e_z tot'};
276 v1 = L_band'; v2 = R_band_average'; v3 = L_band_strain'; v4=V_total'; v5=
    p_external'; v6=p_wall'; v7 = (p_wall-p_external)'; v8=A_band';v9=
    Wall_force'; v10=External_force'; v11 = R_band_strain', v12=e_r', v13=e_z
    ', v14=e_r_total', v15=e_z_total';
277 fid = fopen('abc.txt','wt');
278 fprintf(fid, '%s ', column_names{:});
279 fprintf(fid, '\n');
280 block_of_data = [v1, v2, v3, v4,v5,  v6, v7, v8, v9, v10, v11, v12, v13, v14,
     v15];
281 fmt = repmat('%15g ', 1, 15);
282 fmt(end:end+1) = '\n';
283 fprintf(fid, fmt, block_of_data.');   %transpose is needed to get everything
    right
284 fclose(fid);
285
286 %Figure 2: shear modulus: 0.5*p_wall_min_p_ vs. eps_r-eps_z
```

```
overgang_shear2 = N_images;   %Insert the number of images which must be used for the first slope

p1=polyfit((e_G_(1:overgang_shear2))./2,p_difference(1:overgang_shear2 )./2,1);
a1=p1(2); b1=p1(1);
p2 =polyfit((e_G_(overgang_shear2:N_images))./2,p_difference(overgang_shear2:(N_images))./2,1);5
a2=p2(2); b2=p2(1);
figure(2)
hold on;
clf reset;
plot((e_G_(1:N_images ))./2,p_difference(1:N_images )./2,'r.',(e_G_(1:overgang_shear2))./2,a1+b1*(e_G_(1:overgang_shear2))./2,'b--','MarkerSize',10,'LineWidth',1.5);
hold on
plot((e_G_(overgang_shear2-1:(N_images) ))./2,a2+b2*(e_G_(overgang_shear2-1:(N_images)))./2,'b--','MarkerSize',10,'LineWidth',1.5);

axis square; axis on;
h=legend(' ',['slope 1: ',num2str(round(b1)),' Pa'],['slope 2: ',num2str(round(b2)),' Pa'],'Location','northwest' ,3);
%h=legend(' ',['slope: ',num2str(round(b1)),' Pa'],'Location','northwest', 2);
set(h,'Box','off');
set(gca,'Box','on');
set(gca,'FontSize',14);
set(gca,'LineWidth',2);
set(gca,'FontName','Times');
xlabel('$$\epsilon_{r} - \epsilon_{z}$$','fontsize',24, 'interpreter','latex');
ylabel('$$(p_\mathrm{wall} - p$$)/2 [Pa]','fontsize',24, 'interpreter','latex');
title('Shear modulus. z: only middle part, r: R_{average}')

curr_fig=figure(2);
Image = getframe(curr_fig);
saveas(h,'G_plot_middle.fig','fig');
saveas(h,'G_plot_middle.pdf','pdf');
hold off;

%Figure 3: shear modulus: 0.5*p_wall_min_p_ vs. eps_r-eps_z
overgang_shear = N_images;  %Insert the number of images which must be used for the first slope

p1=polyfit((e_G_2(1:overgang_shear))./2,p_difference(1:overgang_shear )./2,1);
a1=p1(2); b1=p1(1);
p2 =polyfit((e_G_2(overgang_shear:(N_images)))./2,p_difference(overgang_shear:(N_images) )./2,1);
a2=p2(2); b2=p2(1);
figure(3)
hold on;
clf reset;
plot((e_G_2(1:N_images ))./2,p_difference(1:N_images )./2,'r.',(e_G_2(1:overgang_shear))./2,a1+b1*(e_G_2(1:overgang_shear))./2,'b--','MarkerSize',10,'LineWidth',1.5);
hold on
plot((e_G_2(overgang_shear:(N_images) ))./2,a2+b2*(e_G_2(overgang_shear:(N_images)))./2,'b--','MarkerSize',10,'LineWidth',1.5);
```

```
331
332 axis square; axis on;
333 h=legend(' ',['slope 1: ',num2str(round(b1)),' Pa'],['slope 2: ',num2str(
        round(b2)),' Pa'],'Location','northwest' ,3);
334 %h=legend(' ',['slope: ',num2str(round(b1)),' Pa'], 'Location','northwest',
        2);
335 set(h,'Box','off');
336 set(gca,'Box','on');
337 set(gca,'FontSize',14);
338 set(gca,'LineWidth',2);
339 set(gca,'FontName','Times');
340 xlabel('$$\epsilon_{r} - \epsilon_{z}$$','fontsize',24, 'interpreter','latex'
        );
341 ylabel('$$(p_\mathrm{wall} - p$$)/2 [Pa]','fontsize',24, 'interpreter','latex
        ');
342 title('Shear modulus. z: total cell length, r: R_{average}')
343
344 curr_fig=figure(3);
345 Image = getframe(curr_fig);
346 saveas(h,'G_plot_total.fig','fig');
347 saveas(h,'G_plot_total.pdf','pdf');
348 hold off;
349
350 %Figure 4: compression modulus: p_average vs. V_strain = (2*p_wall+p)/3 vs dV
        /V
351 overgang_compression = N_images;    %Insert the number of images which must
        be used for the first slope
352
353 p1=polyfit((V_strain_(1:overgang_compression )),p_average(1:
        overgang_compression ),1);
354 a1=p1(2); b1=p1(1);
355 p2=polyfit((V_strain_(overgang_compression:(N_images))),p_average(
        overgang_compression:(N_images)),1);
356 a2=p2(2); b2=p2(1);
357 figure(4);
358 hold on;
359 clf reset;
360 plot((V_strain_(1:N_images )),p_average(1:N_images ),'r.',(V_strain_(1:
        overgang_compression )),a1+b1*(V_strain_(1:overgang_compression )),'b--',
        'MarkerSize',10,'LineWidth',1.5);
361 hold on
362 plot((V_strain_(overgang_compression:(N_images) )),a2+b2*(V_strain_(
        overgang_compression:(N_images) )),'b--','MarkerSize',10,'LineWidth',1.5)
        ;
363
364 axis square; axis on;
365 h=legend(' ',['slope 1: ',num2str(round(b1)),' Pa'],['slope 2: ',num2str(
        round(b2)),' Pa'],'Location','northwest' ,3);
366 %h=legend(' ',['slope: ',num2str(round(b1)),' Pa'], 'Location', 'northwest
        ',2);
367 set(h,'Box','off');
368 set(gca,'Box','on');
369 set(gca,'FontSize',14);
370 set(gca,'LineWidth',2);
371 set(gca,'FontName','Times');
372 xlabel('$$dV/V$$','fontsize',24, 'interpreter','latex');
373 ylabel('$$(2p_\mathrm{wall} + p)/3$$ [Pa]','fontsize',24, 'interpreter','
        latex');
374 title('Compression modulus')
375
```

```
376 curr_fig=figure(4);
377 Image = getframe(curr_fig);
378 saveas(h,'K_plot.fig','fig');
379 saveas(h,'K_plot.pdf','pdf');
380 hold off;
```